HHS Public Access

Author manuscript

Cell Metab. Author manuscript; available in PMC 2024 April 23.

Published in final edited form as:

Cell Metab. 2023 July 11; 35(7): 1147–1162.e7. doi:10.1016/j.cmet.2023.05.008.

Ketogenic diet promotes tumor ferroptosis but induces relative corticosterone deficiency that accelerates cachexia

Miriam Ferrer[1,2], **Nicholas Mourikis**[1], **Emma E. Davidson**[1], **Sam O. Kleeman**[1], **Marta Zaccaria**[3], **Jill Habel**[1], **Rachel Rubino**[1], **Qing Gao**[1], **Thomas R. Flint**[4], **Lisa Young**[4], **Claire M. Connell**[4], **Michael J. Lukey**[1], **Marcus D. Goncalves**[5], **Eileen P. White**[6], **Ashok R. Venkitaraman**[2,7,8], **Tobias Janowitz**[1,9,*]

[1]Cold Spring Harbor Laboratory, Cold Spring Harbor, NY 11724, USA

[2]MRC Cancer Unit, University of Cambridge, Cambridge Biomedical Campus, Cambridge CB2 0XZ, UK

[3]University College London, London WC1E 6BT, UK

[4]Department of Oncology, CRUK Cambridge Institute, Cambridge Biomedical Campus, Cambridge CB2 0RE, UK

[5]Division of Endocrinology, Department of Medicine, Weill Cornell Medicine, New York, NY 10021, USA

[6]Department of Molecular Biology and Biochemistry, Rutgers Cancer Institute of New Jersey, New Brunswick, NJ 08901, USA; Ludwig Princeton Branch, Ludwig Institute for Cancer Research, Princeton University, Princeton, NJ 08544, USA

[7]Cancer Science Institute of Singapore, National University of Singapore, Singapore 117599, Singapore

[8]Institute for Molecular & Cell Biology, Agency for Science, Technology and Research (A*STAR), Singapore 138648, Singapore

[9]Northwell Health Cancer Institute, Northwell Health, New Hyde Park, NY 11042, USA

SUMMARY

The dependency of cancer cells on glucose can be targeted with high-fat low-carbohydrate ketogenic diet (KD). However, hepatic ketogenesis is suppressed in IL-6 producing cancers, which prevents the utilization of this nutrient source as energy for the organism.

In two IL-6 associated murine models of cancer cachexia we describe delayed tumor growth but accelerated onset of cancer cachexia and shortened survival when mice are fed KD. Mechanistically, we find this uncoupling is a consequence of the biochemical interaction of

*Correspondence: janowitz@cshl.edu (T.J.).

AUTHOR CONTRIBUTIONS

Conceptualization, M.F. and T.J.; Methodology, M.F., A.R.V., T.J.; Investigation, M.F., N.M., E.E.D., S.O.K., M.Z., J.H, R.R., T.R.F., L.Y., C.M.C., and M.L.; Writing – Original Draft, M.F.; Writing – Review & Editing, all authors.; Project Administration, M.F.; Funding Acquisition, M.F., A.R.V. and T.J.; Resources, A.R.V. and T.J.; Supervision, T.J.

DECLARATION OF INTERESTS

The authors declare no competing interests.

two simultaneously occurring NADPH-dependent pathways. Within the tumor, increased lipid peroxidation and, consequently, saturation of the glutathione (GSH) system leads to ferroptotic death of cancer cells. Systemically, redox imbalance and NADPH depletion impairs the biosynthesis of corticosterone, the main regulator of metabolic stress, in the adrenal glands. Administration of dexamethasone, a potent glucocorticoid, increases food intake, normalizes glucose levels and utilization of nutritional substrates, delays onset of cancer cachexia and extends survival of tumor-bearing mice fed KD, while preserving reduced tumor growth.

Our study highlights that the outcome of systemic interventions cannot necessarily be extrapolated from the effect on the tumor alone, but that they have to be investigated for anti-cancer and host effects. These findings may be relevant to clinical research efforts that investigate nutritional interventions such as KD in patients with cancer.

Graphical Abstract

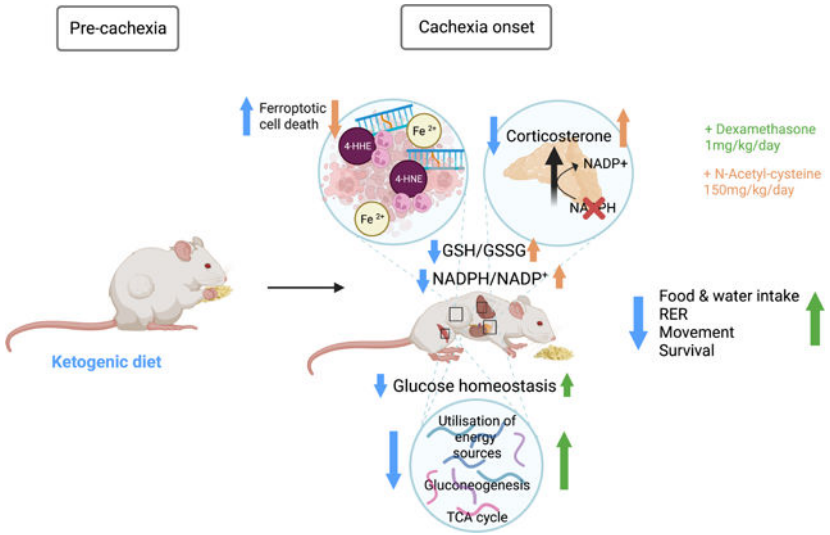

INTRODUCTION

Cancer, at a cellular and organismal level, is at least in part a metabolic disease. Cancer cells have altered metabolism to accommodate nutrient demand and maintain growth and proliferation. For example, they frequently rely on increased glucose consumption to supply anabolic metabolism [1]. At a systemic level, cancer can alter the metabolism of the host by inducing profound changes in nutrient intake and handling that culminate in cachexia. Cancer cachexia is a severe wasting syndrome characterized by reduced food intake and terminal weight loss that affects up to 80% of all patients with cancer [2], and causes significant morbidity and mortality [3]. This persistent metabolic stress condition increases glucocorticoid levels in humans and mouse models of cancer cachexia.

The dependency of cancer cells on glucose has been targeted by utilization of ketogenic diets (KD) containing high fat and low carbohydrate levels. KDs are explored as therapeutic intervention in end-stages of cancer that are associated with cachexia [4]. Several studies report an anti-inflammatory and a delayed tumor growth effect of KD in pre-clinical models

[5–7] and in humans [8]. However, hepatic ketogenesis is suppressed in murine models of IL-6-secreting cancers that ultimately cause cancer cachexia [9,10]. This results in an inability of the organism to metabolize the lipid-rich KD into survival-sustaining energy molecules. Together, this scenario raises the question whether the inability of the cancer cell or the organism to utilize the macronutrients supplied by KD is dominant with regard to outcome.

Lipid peroxidation is a non-enzymatic route of fatty acid metabolism that is oxygen radical-dependent [11,12]. Metabolism of unsaturated lipids through non-enzymatic lipid peroxidation is a recognized source of highly reactive molecules named lipid peroxidation products (LPPs), such as 4-hydroxynonenal (4-HNE), 4-hydroxyhexenal (4-HHE), and malondialdehyde (MDA), that cause cross-linkage on DNA and proteins through the formation of etheno-adducts [13,14]. Under physiological conditions, lipid peroxidation rates are low and non-toxic since lipid hydroperoxides (LOOHs) are quickly removed from cells by constitutive antioxidants defense systems such as the NADPH-dependent glutathione (GSH) system [15,16]. When this detoxification fails, the accumulation of LPPs results in a type of programmed cell death dependent on iron that is termed ferroptosis [17].

Cortisol is the major human glucocorticoid, equivalent to corticosterone in rodents. Cortisol release is part of the physiological response to starvation in cancer cachexia that drives adaptive pathways and regulates nutrient storage, glucose levels, protein breakdown, and lipolysis [18–20]. Biosynthesis of glucocorticoids occurs in the cortex of the adrenal glands through repeated NADPH-dependent enzymatic reduction of cholesterol. This process is under the control of the hypothalamic-pituitary-adrenal (HPA) axis. The inability to mount an adequate stress response due to irreversible damage to the adrenal cortex (e.g., auto-immunity) [21] or pharmacotherapy-induced suppression of the HPA axis [22] presents a life-threatening condition called adrenal insufficiency.

Therefore, glucocorticoid synthesis and the LOOH detoxification pathway share the requirement for NADPH as cofactor, yet their biochemical interdependency has not been explored. This interaction becomes relevant when both pathways simultaneously occur in metabolically stressed organisms (e.g., cachexia) fed a diet with high fat content (e.g., KD).

In this study, we set out to determine the differential effect of KD on tumors and the host organism using two murine models of cancer cachexia. We find that although KD slows tumor growth, it shortens survival by accelerating the onset of cachexia. Mechanistically, increased lipid peroxidation in KD-fed tumor-bearing mice leads to systemic redox imbalance. Within tumors, this results in saturation of the GSH pathway, formation of LPPs and consequent ferroptotic death of cancer cells. Moreover, we discover that NADPH depletion impairs corticosterone biosynthesis in the adrenal cortex, inducing a relative adrenal insufficiency and metabolic maladaptation in mice fed KD. Treatment with the synthetic corticosteroid dexamethasone delays the onset of cancer cachexia and extends survival of tumor-bearing mice fed KD by improving food intake, metabolic homeostasis and utilization of nutritional substrates, while preserving the anti-tumor response.

The uncoupling of tumor growth from overall survival illustrates why clinical trials should monitor the host response to nutritional interventions such as KD closely.

RESULTS

Ketogenic diet delays tumor growth but shortens overall survival in two mouse models of cancer cachexia

To investigate the effect of ketogenic diet on established IL-6-secreting cachexia-inducing cancers and the tumor-bearing host, BALB/c mice bearing subcutaneous C26 colorectal tumors for 14 days, and KPC mice ($Kras^{G12D/+}$;$Trp53^{R172H/+}$;Pdx-1-Cre), a genetically engineered mouse model (GEMM) of pancreatic cancer, with >3–5mm size tumors were challenged with a low-carbohydrate, moderate-protein, high-fat, ketogenic diet (KD) or maintained on normal diet feeding (NF) (Figure S1A and Extended Data Table S1). Tumor growth was significantly decelerated in mice fed KD in both models, indicating a diet-mediated anti-tumor effect (Figures 1A and 1B). However, KD prompted an earlier onset of cancer cachexia (>15% bodyweight loss), thus shortening overall survival (OS) in both C26 and KPC mice fed KD compared to their counterparts fed NF (Median OS: 10 days C26/KD, 14 days C26/NF, 6.5 days KPC/KD, 17 days KPC/NF) (Figures 1C and 1D, Figures S1B and S1C). At endpoint, tumor-bearing mice exhibited loss of subcutaneous and gonadal fat tissue, depletion of quadriceps muscle mass and splenomegaly, all of which are recognized signs of cachexia (Figures S1D and S1E).

Longitudinal monitoring of blood glucose levels showed an acute decrease in glucose of littermate controls (LM) and PC controls after introduction of KD that completely recovered after 24h to similar levels of controls fed NF. In contrast, C26 and KPC tumor-bearing mice on KD did not adapt to the new nutritional source and their glucose levels kept declining over time, reaching the lowest levels at cachectic endpoint. Tumor-bearing mice on NF had lower glucose levels than their non-tumor bearing counterparts but higher than tumor-bearing mice on KD, and they were able to maintain stable glucose measurements until onset of cachexia when the levels dropped abruptly (Figures 1E and 1F). Circulating ketones were significantly increased in all KD fed compared to NF fed groups, but tumor-bearing mice had lower levels compared to their non-tumor bearing control counterparts on the same diet (Figures 1G and 1H). Littermate mice on KD had a 2-fold upregulation of hepatic mRNA levels of PPARα target genes that regulate ketogenesis, *Acadm* and *Hmgsc2*, compared to littermates on NF. The expression was also 2-fold higher than in C26 tumor-bearers on KD, which were unable to upregulate the transcriptional targets responsible for ketogenesis despite the increased dietary substrate. C26 tumor-bearing mice on NF exhibited suppressed transcriptional regulation of ketogenesis compared to NF fed littermates, as previously described [9] (Figures S1F and S1G). Food intake was decreased in both tumor-bearing groups as cachexia developed (Figures S1H and S1I). Taken together, these data demonstrate that KD impairs the metabolic responses that maintain glucose levels in the tumor-bearing host, and does not overcome the maladaptive, tumor-mediated, suppression of ketogenesis.

Ketogenic diet induces formation of etheno-adducts and ferroptotic cell death of cancer cells that can be prevented by NAC

To quantify the NADPH-dependent detoxification of LOOHs and formation of LPPs, and to study the redox state of both the tumor and the host in the context of the lipid-enriched

KD (Extended Data Table S1), we performed an in-depth metabolomics analysis on liver and tumor tissue of tumor-bearing C26 and LM mice fed KD or NF. 4-HNE, the major LPP resulting from oxidation of fatty acids, accumulated in the liver of tumor-bearing C26 mice fed KD compared to NF fed tumor-bearing mice. LM on KD had unchanged levels of 4-HNE in the liver compared to NF fed LM, suggesting its production was efficiently detoxified (Figure 2A and S2A). GSH to GSSG ratio in liver and tumor of C26 tumor-bearing mice on KD was decreased compared to those on NF, suggesting an ongoing utilization of the reductive power of GSH molecules with the purpose of detoxifying LOOHs (Figure 2B and 2C). Tumor metabolomics of C26 mice fed KD or NF were separated by PCA (Figure S2B). The rate-limiting precursor metabolite for GSH biosynthesis, cysteine, was also decreased in tumors from C26 mice fed KD (Figure 2D), whereas ophthalmate, a biomarker for oxidative stress and GSH depletion [23], significantly accumulated in KD tumors (Figure S2C). Other indicators of redox perturbation, such as collapse of the antioxidant carnosine [24] (Figure S2D) and evidence of hypotaurine to taurine oxidation (Figures S2E and S2F) [25] were present in tumors from C26 KD-fed mice. These data are compatible with an increased formation of toxic and highly mutagenic LPPs due to saturation of the GSH pathway in tumors from C26 mice on KD compared to those fed NF. Adduct formation by the LPP 4-HNE was significantly elevated in the tumors from C26 and KPC mice fed KD compared to those fed NF (Figure 2E and 2F). 4-HNE adducts in KD-fed C26 mice were prevented with administration of N-acetyl cysteine (NAC), an antioxidant that boosts GSH biosynthesis, prevents LOOH peroxidation and therefore formation of LPPs (Figures 2E, S2A and S2G).

Accumulation of LPPs results in ferroptosis [26], an iron-dependent cell death that has previously been described in cysteine-depleted tumors [27]. To explore the possibility that ferroptotic cell death in tumors from KD-fed mice is partly responsible for reduced tumor burden and slower tumor growth trajectories, we first performed Oil-Red-O staining of lipids in tumors from C26 mice. C26 mice on KD had significant accumulation of lipid droplets in the tumor, whereas tumors from C26 mice on NF had no evidence of lipid storage (Figure S2H). We next quantified the levels of ferrous (Fe^{2+}/Iron II) and ferric (Fe^{3+}/ Iron III) iron in tumor samples. Ferrous iron is an established indirect marker of ferroptosis and it accumulated in tumors from C26 and KPC mice fed KD, suggesting an ongoing ferroptotic cell death mechanism in these tumors compared to tumors from mice fed NF (Figure 2G and 2H). A dead tumor core was observed in tumors from mice fed KD by hematoxylin and eosin (H&E) staining (Figure 2I). Immunohistochemistry staining of 4-HNE cross-linkage in liver tissue showed increased formation of 4-HNE adducts with both cytoplasmatic and nucleic proteins in hepatocytes of C26 tumor-bearing mice fed KD compared to any other group (Figure 2J and 2K). Moreover, tumors from mice on KD treated with NAC were notably larger than those from untreated mice fed KD (Figure 2L), and ferrous iron levels were depleted upon NAC treatment (Figure 2G), indicating that NAC administration is sufficient to prevent ferroptotic cell death in these tumors. Administration of the ferroptosis inhibitor Liproxstatin-1 [28] to tumor-bearing C26 mice accelerated tumor growth in mice fed KD but had no effect in those fed NF (Figure 2M), corroborating that ferroptotic cell death contributes to the smaller tumor burden observed in mice fed KD. We next performed a pharmacological experiment to recapitulate the effect induced by KD

and validate this hypothesis further. Indeed, administration of RSL3 [29], a specific inhibitor of glutathione peroxidase 4 (GPx4) that blocks the detoxification of LOOHs and thereby induces accumulation of LPPs and cellular ferroptosis, to tumor-bearing mice fed NF led to reduced tumor growth (Figure S2I).

We next set out to validate these findings in the KPC model. RNAseq data from tumors of cachectic KPC mice demonstrated significant overexpression of E2F and Myc targets, major regulators of cellular metabolism in response to stress [30], in tumors from KPC mice fed KD compared to KPC fed NF. The E2F axis has previously been associated with oxidative stress and ferroptosis in neurons, and its silencing leads to prevention of this iron-dependent cell death [31]. Myc signaling has also been linked to mediation of, and sensitization to, ferroptotic cell death [32,33]. Gene expression marking activity of the G2/M checkpoint were significantly upregulated in tumors from KPC mice fed KD, and since the activation of this checkpoint occurs when the DNA is damaged, this suggests that LPP formation in the cancer cells causes DNA crosslinking, adduct formation and consequently cell cycle arrest (Figure S2J).

Apoptosis was disregarded as an additional mechanism contributing to reduced tumor growth in mice fed KD because apoptotic markers such as Caspase-3 were expressed similarly by Western Blot (WB) in C26 tumors from both dietary groups. BAX staining suggested even lower levels of apoptotic cell death in tumors from C26 KD-fed mice compared to those from C26 fed NF (Figure S2K). Cell proliferation, measured by Ki67 staining, was also not affected by the dietary challenge itself (Figure S2L).

All of these findings demonstrate that elevated oxidative stress leading to cell cycle arrest and ferroptotic cell death caused by build-up of LPPs are mechanisms contributing to smaller tumor burden in mice fed KD.

Since ferroptosis is an immunogenic process [34], we next studied the immune infiltration in tumors from KD- and NF-fed mice. We found a positive trend for enrichment of all immune cell types examined in KD tumors, reaching statistical significance for neutrophils (Figures S2M, S2N, S2O and S2P). This observation may be explained by active recruitment of neutrophils to areas undergoing ferroptotic cell death.

Ketogenic diet impairs glucocorticoid synthesis in tumor-bearing mice

Corticosterone is the main glucocorticoid involved in metabolic adaptation under stress conditions in mice, acting as a regulator of metabolic rates and availability of fuel substrates. Metabolic stressors such as caloric restriction associated with cachexia induce high levels of corticosterone [9]. Similar to the detoxification of LOOHs, the corticosteroid synthesis pathway in the cortex of the adrenal gland requires a constant supply of NADPH cofactor molecules (Figure S3A). To gain a deeper understanding of the metabolic stress response in KD and NF fed mice, we quantified circulating levels of corticosterone and cholesterol, the substrate for corticosterone biosynthesis in the adrenals. Control littermates on either diet had baseline levels of corticosterone in circulation. At the time of cachexia, C26 and KPC tumor-bearing mice fed NF displayed a sharp increase in corticosterone concentration, but levels in those fed KD were not elevated in comparison (Figures 3A, 3B and S3B). Cholesterol availability was similar in C26 and KPC mice fed with KD and NF diets

(Figures 3C and 3D) but pregnenolone levels significantly accumulated in the plasma of C26 mice fed KD compared to those fed NF (Figure 3E), pointing towards a defect in the synthetic cascade of corticosterone (Figure S3A) rather than an absence of substrate.

We next compared the transcriptome of the adrenal glands in tumor-bearing KPC mice fed KD or NF, and using Gene Set Enrichment Analysis (GSEA) we found that the steroid biosynthesis and cholesterol homeostasis pathways were significantly downregulated in KPC mice fed KD compared to those fed NF (Figure S3C). These data demonstrate an impaired corticosterone production and inefficient stress response in the adrenal glands of tumor-bearing mice fed KD compared to those fed NF. One of the major actions of aldosterone, a mineralocorticoid hormone derived from downstream processing of corticosterone, is sodium retention. We noted a relative hyponatremia in C26 tumor-bearing mice fed KD compared to those fed NF and LM on either diet (Figures 3F), which may, at least in part, be a result of diminished adrenally-derived mineralocorticoid action. This further supports an impaired hormone biosynthesis in the adrenal glands of these mice.

The adrenal glands are part of the HPA axis. The adrenocorticotropic hormone (ACTH) is a hormone produced by the pituitary gland that drives corticosterone production in the adrenal glands. Elevated circulating corticosterone levels induce negative feedback on the HPA axis and inhibit ACTH release. In order to assess whether the impaired synthesis of corticosterone in tumor-bearing mice fed KD is a) a localized phenomenon in the cortex of the adrenal glands, b) due to an upstream defect in the HPA axis, such as inadequate ACTH production by the pituitary gland, or c) a combination of both, we quantified ACTH in the plasma of C26 mice and LM fed NF or KD. At endpoint, levels of ATCH detected in cachectic tumor-bearing mice were more broadly distributed compared to levels seen in non-tumor-bearing control mice, and there was a small but significant increase in ACTH in C26 KD-fed mice compared to those NF-fed, suggestive again that the primary issue pertaining to this relative corticosterone deficiency was sited within the adrenal glands (Figure 3G). However, given the variance in ACTH levels, a minor contribution from upstream mechanisms to the observed hypocorticosteronemia cannot be excluded.

Since corticosterone release can potentially be driven by direct stimulation of the adrenal glands by non-ACTH peptides such as IL-6 [35–37], and the C26 model is known to display high IL-6 levels [9], we quantified circulating levels of this cytokine. No diet-mediated differences between the tumor-bearing groups were observed (Figure S3D), indicating that IL-6 does not contribute to the relative corticosterone deficiency observed in KD-fed tumor-bearing mice.

To asses adrenal gland responsiveness, we undertook ACTH stimulation tests using synthetic ACTH (synacthen test) at two timepoints: the first cohort was studied four days after diet change (day18 post-C26 injection), and a second cohort was studied at the onset of cachexia. On day 4 after diet switch, both tumor-bearing C26 groups had higher baseline corticosterone levels compared to LM. In response to ACTH administration, tumor-bearing C26 mice on NF had a stronger response to ACTH than their LM on NF. Conversely, corticosterone upregulation in tumor-bearing C26 mice on KD was significantly reduced compared to the response of LM on KD (Figure 3H). Thus, our results show signs of

malfunction of the stress axis in tumor-bearing mice fed KD even at this early stage. At cachexia endpoint, baseline corticosterone levels pre-stimulation were significantly elevated in tumor-bearing C26 mice on NF compared to those on KD (Figure 3I). Upon ACTH injection, plasma corticosterone increased over time in tumor-bearing C26 mice fed NF and in LM, while levels in tumor-bearing C26 mice fed KD did not significantly change. After 60 minutes, levels of corticosterone in tumor-bearing C26 mice fed NF were almost 2.5-fold higher than in those fed KD. Both LM groups showed similar responses and reached peak levels comparable to those of tumor-bearing C26 mice on NF at baseline (Figure 3I). These data point towards an intrinsic difficulty in the adrenal glands of KD-fed tumor-bearing mice to respond to hormonal stimulation and release corticosterone compared to NF-fed tumor-bearing mice. Together, we provide evidence that KD drives the development of a relative adrenal insufficiency in tumor-bearing mice.

NAC treatment rescues corticosterone synthesis in tumor-bearing mice fed ketogenic diet

In order to identify the mechanism underlying the relative deficiency in corticosterone biosynthesis in tumor-bearing mice fed KD, we next explored the interaction of the GSH pathway (Figure S2A) and the corticosterone synthesis pathway (Figure S3A) through their common need of NADPH sources. Targeted quantification of NADPH and NADPH/NADP+ ratio in the adrenal glands of cachectic mice and controls showed higher levels of NADPH in tumor-bearing C26 mice fed NF compared to LM fed NF, as it would be anticipated in the context of an ongoing release of corticosterone. However, NADPH levels and the NADPH/NADP+ ratio were diminished in the adrenal glands of C26 mice fed KD compared to C26 mice fed NF. Administration of NAC, a cysteine prodrug that replenishes intracellular GSH levels in the absence of NADPH consumption, rescued NADPH levels and the NADPH/NADP+ ratio in these mice (Figure 4A and S3E). Of note, NADP(H) are challenging targets for quantitative analysis due to their transient nature and chemical instability during sample extraction and processing, which is reflected in the variance of measurements within groups. Nevertheless, taken together, these data indicate that the increased demand for NADPH in the process of detoxification of LOOHs leads to a shortage of this cofactor, which then is not available for use in the synthesis of corticosterone and leads to low levels of this stress hormone in tumor-bearing mice fed KD.

To examine this hypothesis further, we measured corticosterone levels in tumor-bearing mice fed KD or NF and treated with NAC. Circulating corticosterone was markedly higher in the NAC-treated groups compared to untreated and control groups on the same diet (Figure 4B). Simultaneously, pregnenolone accumulation in KD-fed tumor-bearing mice was no longer detected upon NAC treatment (Figure 4C), indicating conversion of this early intermediate to downstream intermediates of corticosterone biosynthesis and ultimately to corticosterone. Therefore, promoting GSH production through NAC diminishes the need of NADPH oxidation, consequently increasing GSH's LOOH-detoxifying activity and preventing NADPH depletion. NADPH availability enables an appropriate synthesis of corticosterone in the adrenals and leads to the physiological rise in systemic corticosterone levels in the context of metabolic stress associated with cachexia.

LPPs exposure decreases cortisol production in a human adrenal cortex-derived cell line

After their production, LPPs react with intracellular proteins and DNA. They are enzymatically reduced via phase I (ALDH, AOR, AKR, CYPs) and phase II (GSH) metabolism, and these reductive reactions are NADPH-dependent [38]. We next implemented the human adrenal cortex-derived cell line, H295R, to test the direct effects of LPPs on cortisol synthesis *in vitro*. We first identified doses of 4-HNE, 4-HHE and MDA that did not affect viability of H295R cells upon exposure (Figure 4D, 4E and 4F). Single or daily treatment of H295R cells with tolerated doses of 4-HNE, 4-HHE or MDA, led to lower cortisol production after 48h and 72h compared to the cortisol levels released to the media by untreated adrenocortical cells (Figure 4G, 4H and 4I). Thus, these data suggest that LPPs can directly suppress cortisol production in adrenocortical human cells, most likely due to a NADPH-depleting effect similar to the one observed *in vivo*.

GDF-15 is elevated in cachexia and increased by ketogenic diet

While the KD-mediated biochemical impairment of the adrenal glands stress response and resulting defective glucocorticoid biosynthesis in tumor-bearing mice described above can account for shortened survival, it does not necessarily explain reduction in food intake. GDF-15, a TGF-beta superfamily member that is produced by cells under stress, mediates reduced food intake by binding its cognate receptor GFRAL in the area postrema[39]. It has been implemented in the anorectic response in cancer cachexia [40], and in aldehyde toxicity-induced anorexia [41]. In keeping with these findings, we observed elevated circulating GDF-15 levels in cachectic NF-fed C26 mice, which were further elevated in cachectic KD-fed mice (Figure 5A), reflecting the systemic oxidative and metabolic stress of the organism and explaining at least in part the reduced food intake observed in the cachectic phase of the disease (Figure S1F and S1G).

Appropriate usage of energy sources in the context of cachexia is impaired in ketogenic diet-fed tumor-bearing mice

To test the relevance of glucocorticoid-driven metabolic adaptation that promotes survival in the context of a cachectic tumor-bearing host and the impact that its malfunction may have, we assessed and compared the systemic metabolic state of NF- and KD-fed mice.

At endpoint, tumor-bearing mice exhibited signs of cachexia, including splenomegaly, and loss of fat and muscle mass (Figure S1D and S1E). Atrogin-1 and MuRF1 are markers of skeletal muscle atrophy and proteolysis [42]. mRNA quantification exhibited upregulated expression of these two muscle-specific E3 ubiquitin ligases in the quadriceps of cachectic C26 mice compared to LM controls, yet the fold increase was significantly less pronounced in tumor-bearing KD-fed than in NF-fed mice (Figures 5B and 5C). Creatinine, an end product of muscle catabolism, was markedly increased in the circulation of cachectic tumor-bearing C26 and KPC mice fed NF but not in those fed KD (Figures 5D and 5E), presumably as a consequence of lower corticosterone levels that regulate the breakdown of proteins. Urea production is commonly upregulated in cachexia due to increased protein release from muscle tissue breakdown [43,44], however, urea levels stayed low in cachectic tumor-bearing mice fed KD compared to those fed NF (Figures S4A and S4B). These

observations indicate that the process of ubiquitin-mediated proteolysis is impaired in cachectic mice fed KD despite exhibiting cachexia-associated muscle atrophy.

We next examined the hepatic response to metabolic stress in cachectic tumor-bearing mice undergoing systemic wasting and decreased food intake. RNAseq data from livers of cachectic KPC mice demonstrated downregulated genes related to hepatic glycolysis, glucose metabolism and pyruvate metabolism in KD-fed compared to NF-fed KPC, many of which are glucocorticoid response genes (Figure 5F). Peroxisomal lipid metabolism and fatty acid metabolism appeared upregulated in the liver of tumor-bearing KPC mice fed KD, in agreement with a lipid-rich diet (Figure 5G). Moreover, untargeted liver metabolomics in LM and tumor-bearing C26 mice on KD or NF diets manifested distinct hepatic metabolic profiles (Figure S4C). Specific pathway analysis led us to identify a marked accumulation of fatty acid metabolites in the liver of tumor-bearing C26 mice fed KD compared to those fed NF (Figure 5H). These data, together with the observation of macroscopically larger liver sizes (Figure S1D), suggested that inappropriate utilization of lipids could account for the reduced glucose levels and the hepatic build-up of unprocessed fat in tumor-bearing mice on KD. In addition, intermediates of the tricarboxylic acid (TCA) cycle appeared upregulated in the liver of tumor-bearing NF-fed C26 mice compared to those KD-fed (Figure 5H). The TCA cycle in hepatic cells is the metabolic progenitor pathway for gluconeogenesis and the main source of energy for the body [45,46]. Glycerol and amino acids such as glutamine and arginine are a major cellular carbon source for oxidative catabolism via the TCA cycle. These energy substrates were elevated in the liver of tumor-bearing C26 mice fed KD (Figure 5I, 5J and 5K), reinforcing the idea of impaired metabolic activity and deficient energy production in these mice.

Altogether, these data provide evidence that lack of appropriate corticosterone biosynthesis in tumor-bearing mice fed KD is associated with metabolic maladaptation, inability to use energy sources, reduced glucose levels, and ultimately earlier onset of cancer cachexia.

Dexamethasone treatment extends survival and improves metabolic adaptation of tumor-bearing mice fed ketogenic diet

Given the relevance of corticosterone in metabolic adaptation and efficient energy utilization under stress conditions such as cancer cachexia, we next tested the hypothesis that the survival disadvantage in tumor-bearing mice fed KD is driven by their restricted corticosterone production.

BALB/c mice bearing C26 tumors for 14 days were either fed KD or NF and treated daily with 1mg/kg of Dexamethasone intraperitoneally. Dexamethasone is a synthetic long-acting potent glucocorticoid analogue, with a glucocorticoid activity of 30 relative to cortisol [47,48]. Treatment with Dexamethasone significantly extended OS in tumor-bearing C26 mice fed KD compared to all other tumor-bearing groups fed with either diet (Median OS: 10 days C26/KD, 33 days C26/KD + Dex, 14 days C26/NF, 19 days C26/NF + Dex). Specifically, Dexamethasone led to a delayed onset of cachexia (>15% bodyweight loss) in both diet groups but most effectively in KD-fed C26 mice (Figure 6A, Figure S5B). Moreover, Dexamethasone prompted faster tumor growth thereby shortening progression free survival (PFS) (time until tumor size >2000 mm^3) in NF-fed, but not in KD-fed, C26

mice (Figures 6B and S5C). At endpoint, tumor burden in Dex-treated KD-fed C26 mice remained unchanged whereas tumors in Dex-treated NF-fed C26 mice increased ~2-fold in weight (Figure 6C). Increased formation of 4-HNE adducts in the tumors of Dex-treated KD-fed C26 mice but not in those NF-fed (Figure 6D) suggests that differences in tumor burden are attributable to KD-induced ferroptotic cell death.

After only 4 days of treatment, Dexamethasone rescued the early depletion of fat tissue induced by KD in tumor-bearing animals, but NF-fed C26 mice showed no differences in fat tissue (Figure 6E). This is in agreement with hepatic metabolomics at endpoint, which suggest a decrease of lipolysis in the liver of Dex-treated KD-fed C26 tumor-bearing mice compared to untreated KD-fed C26 mice, and unchanged hepatic fatty acid metabolism in NF-fed mice on Dexamethasone (Figure S5D). Quadriceps and liver mass were not affected by Dexamethasone whereas splenic size was reduced in both treated C26 tumor-bearing groups, probably as a consequence of the immunosuppressive effects of Dexamethasone (Figure S5E). Moreover, Dexamethasone increased circulating glucose levels (Figure 6F), hepatic gluconeogenesis and TCA cycle activity (Figure 6G and 6H) in KD-fed C26 tumor-bearing mice, therefore improving systemic metabolic adaptation that may ultimately be responsible for extending survival of these mice.

To characterize further the metabolic changes induced by corticosteroids during cancer progression and cachexia, we placed KD- and NF-fed LM controls and tumor-bearing C26 mice, untreated or treated daily with 1mg/kg of Dexamethasone, in metabolic cages capable of precise monitoring of multiple metabolic parameters (details in Methods). The Respiratory Exchange Ratio (RER) is a ratio between the volume of CO_2 produced and the amount of O_2 consumed by the body. A RER value close to 1.0 depicts the use of carbohydrates as energy source, whereas a 0.7 ratio is indicative of fatty acids used as primary fuel [49]. RER values of NF-fed LM fluctuated from 0.9 at night, indicating predominant carbohydrate use, to 0.75 during light hours, when mice tend to sleep and rely on internal fuel sources (Figure 6I). KD-fed LM exhibited RER values around 0.7 throughout the circadian period, in keeping with consumption and metabolism of a lipid-rich diet. As cachexia developed in NF-fed C26 mice, the RER values flattened, as compared to LM on the same diet. This finding is in line with the reduction in food intake and depletion of adipose tissue, which is likely being consumed as fuel (Figure 6E, 6I, and 6J). Cachectic KD-fed C26 mice had very low levels of RER (~0.65) with no diurnal fluctuations (Figure 6I), consistent with a state of prolonged nutrient starvation (Figure 6J). However, treatment of KD-fed C26 mice with Dex increased food intake (Figure 6J), elevated RER, and restored its normal diurnal variation (Figure 6I). These findings associated with a preservation of adipose tissue and reduced markers of hepatic fatty acid metabolism (Figure 6E and S5D). Dexamethasone also increased food intake in NF-fed C26 mice and advanced the phase of the circadian rhythmicity, resulting in a shift that was almost opposed to that of LM and untreated NF-fed C26 mice (Figure 6I).

Next, we examined the effects of cancer, diet, and Dexamethasone on total energy expenditure (TEE). TEE displayed a linear relationship with body weight, as previously reported [50]. Cachectic mice from both the NF and KD diet groups bearing C26 tumors had decreased TEE, as compared to the respective LM counterparts (Figure 6K and 6L). Physical

activity is a key contributor to TEE and it too was found to be low in tumor-bearing mice on both diets (Figure S5G). The KD fed mice had higher TEE than those fed NF for both LM and C26 groups (Figure 6K and 6L). The combination of lower food and water intake (Figure 6J and S5G) and higher TEE (Figure 6K and 6L) may explain why KD-fed C26 mice lose weight more quickly than NF-fed C26 mice. Dexamethasone treatment delayed weight loss and preserved organ mass in KD-fed C26 mice (Figures 6E and S5A). These beneficial effects were associated with a large rise in food intake and a corresponding increase in TEE, physical activity, and RER, suggesting the food is being effectively metabolized. In the NF-fed C26 mice, Dexamethasone increased food intake without a rise in TEE, physical activity, RER, nor the abundance of hepatic TCA intermediates, which suggests defects in nutrient absorption or metabolism (Figure 6J, 6K, 6L and S5F).

In combination, these results are consistent with a systemic role of glucocorticoids in counteracting cachexia-induced metabolic changes by coordinating adaptive metabolic, feeding and behavioral responses in order to promote survival. Furthermore, the well-known immunosuppressive side effect of glucocorticoid drugs becomes detrimental in the context of a carbohydrate-based diet because it prompts immune escape and consequently rapid tumor growth[9], yet this effect is not observed when glucocorticoids are pulsed in combination with a lipid-rich, low-carbohydrate diet that induces ferroptotic death of cancer cells. Altogether, this data supports a synergistic benefit of combining cancer-targeted nutritional interventions with systemic approaches that ameliorate cancer cachexia.

DISCUSSION

In this study, we find that KD uncouples tumor progression from survival in murine models bearing IL-6-associated tumors that impair hepatic ketogenesis [9]. Mechanistically, this fat-enriched diet enhances the production of LOOHs, saturating the GSH pathway and depleting NADPH stores while leading to the accumulation of LPPs. This induces elevation of the stress-induced appetite suppressant GDF-15. In addition, insufficiency of NADPH cofactor leads to a biochemically-induced relative hypocorticosteronemia and, consequently, metabolic maladaptation in response to stress and earlier onset of cancer cachexia. Dexamethasone administration increases food intake, systemic metabolism, and ultimately, extends survival of tumor-bearing mice fed KD.

These findings caution against a universal utilization of delayed tumor growth as a predictor of prolonged survival in cancer models and in the clinic. Disruption in metabolic homeostasis causes poor prognosis and early death of patients with cancer [51], suggesting that therapeutic support of host metabolic adaptation may extend lifespan. Indeed, we find that rescue of the systemic metabolic adaptation (KD+Dex) suppresses cancer cachexia and extends survival without altering tumor burden, indicating that it is the systemic metabolic imbalance that is most lethal. Moreover, targeting metabolic dependency of cancer cells shows therapeutic promise in stalling or delaying tumor growth. However, our results show that careful consideration of this paradigm is indicated, if a chosen nutritional intervention challenges both the metabolism of the organism and the tumor. This is specifically the case for KDs, which are currently tested in clinical trials. Here, the anti-cancer effect may be offset by the inability of the organism to utilize the lipid nutrients, because reprogramming

of systemic metabolism, muscle and fat loss, and reduced food intake are hallmarks of cancer progression and cachexia [52].

Glucocorticoids, and specifically cortisol, regulate metabolism in conditions of stress. Dexamethasone is a corticosteroid commonly used as supportive care for patients with cancer undergoing standard care in order to lower the immune response, reduce inflammation and prevent or treat cancer-related conditions such as anemia, cerebral oedema, hypersensitivity, hypercalcemia and thrombocytopenia. Side effects of Dexamethasone treatment include weight gain, increased glucose levels and fat accumulation. However, our study shows that what would normally be considered in the clinic as metabolic aftereffects of Dexamethasone may become beneficial for pre-cachectic organisms on a fat-rich diet that exhibit metabolic imbalance and inadequate response to preserve glucose levels (e.g., HPA axis unresponsiveness).

Moreover, some preclinical studies and clinical trials suggest that corticosteroid-induced immunosuppression might dampen the activity of cancer chemo-immunotherapy and increase risk of cancer recurrence [53–55], but this is contradicted by others [56,57]. This ongoing debate on the potential impact of corticosteroids on the anti-tumor immune response is illustrated in our preclinical work, as we observe that Dexamethasone administration reduces PFS in NF-fed mice while tumor growth in KD-fed mice is unaffected by Dexamethasone. Thus, the patients' dietary intake and nutritional state may be cofounding factors in clinical trials that investigate the immunosuppressive impact of corticosteroids co-treatment in cancer. Nutritional interventions combined with the minimum effective dose of corticosteroids should be preferred.

Dietary interventions can be used to enhance anti-cancer therapy and improve clinical outcomes [58–60]. Cancer cells exhibit high dependency on glucose [1], which can be exploited by specific diet regimens. Diets can also have an effect on the immune system and influence the anti-tumor response. KDs have been previously studied in patients with cancer and shown to be safe, feasible, and even to have anti-cancer effects. These low-carbohydrate diets reduce circulating glucose levels and suppress pro-tumorigenic mitogens, which combine to limit tumor nutrient uptake. In this study, we show evidence that supports that KD may be slowing down tumor growth not only via nutrient deprivation but also through an ongoing accumulation of LPPs that induces ferroptotic cell death within the tumor. The amino acid composition of the KD (Extended Data Table S1) may also be contributing to the observed phenotype, as the 9-fold decrease in cystine intake can induce ferroptosis independently of fatty acids [27], and the changes in metabolism and energy expenditure of KD-fed mice could be partially attributed to a decrease in methionine intake [61].

We note that the effect of KD on the host is likely context-dependent: it is detrimental for both the tumor and the host that has been metabolically reprogrammed by the established tumor; but KD has no impact on non-tumor-bearing organisms that are able to adapt their metabolism to the nutritional intake. Even if they grow a tumor later on while on KD, the tumor-induced metabolic reprogramming is delayed due to its decelerated growth. This explains differential results in the literature [62], and evidences the importance of dosing and timing in the clinic.

Without independent validation of our results, it is perhaps too early to suggest that KD and glucocorticoid co-administration may be a therapeutic strategy for patients with IL-6-elevating cancers. Translational studies may find that the relative adrenal insufficiency may only be subclinical in humans, because our preclinical study shows lack of an appropriate upregulation of cortisol in the context of metabolic stress, not a complete absence of the hormone. Thus HPA axis activity should be assessed in patients with a lipid-rich nutritional intake, since this may have effects in systemic metabolism and therapeutic outcome, even in asymptomatic patients.

Nevertheless, the reduced tumor growth and prolonged survival of Dex-treated KD-fed mice compared to NF-fed mice with or without Dexamethasone is an encouraging finding. A limitation to this concept is a lack of the exact understanding of how glucocorticoids rescue metabolism in the context of a reprogrammed organism challenged with KD. While this may limit the ability for longitudinal monitoring of the molecular response in patients on the combination intervention, weight trajectories and glucose levels may be suitable and readily obtainable biomarkers for clinical studies.

CONCLUSION

Our study highlights that the effect of systemic interventions cannot necessarily be extrapolated from the effect on the tumor alone, but that they have to be investigated for anti-cancer and host effects. In model systems with established tumors that elevate IL-6, the opposing effect of KD on delayed tumor growth and induction of cachexia leads to a dominant negative effect on survival. These findings may be relevant to clinical research efforts that investigate the potential benefit of KD for patients with cancer.

Limitations of Study

This study implemented model systems of colorectal and pancreatic cancer that are known to recapitulate clinical disease progression from early cancer to cachexia, but clinical validation of our work is needed. We acknowledge that not all cancers lead to IL-6 elevations and therefore cannot comment on the transferability of our findings to other cancers. The time-course of disease progression and metabolic reprogramming in patients with cachexia-inducing tumors has not yet been resolved. We here focus on murine models with fully established tumors that are challenged with KD once metabolic reprogramming has occurred. Future studies have to guide how preclinical work like this is best translated to clinical cancer progression, and how this alignment could guide stratified enrolment of patients into interventional trials. Our work also provides no definitive answer on dosing for glucocorticoid replacement and, here too, detailed clinical studies are required to define the best therapeutic dose range.

STAR METHODS

RESOURCE AVAILABILITY

Lead contact—Further information and requests for resources and reagents should be directed to and will be fulfilled by the lead contact, Tobias Janowitz (janowitz@cshl.edu).

Materials availability—This study did not generate new unique reagents.

Data and code availability

- RNA-seq data have been deposied at GEO and SRA and are publicly available as of the date of publication. Accession numbers are listed in the key resources table.
- This paper does not report original code. Unprocessed data underlying the display items in the manuscript, related to Figures 1–6 and S1–S5 are available as Data S1 - Source data. Supplemental table and figures are available as supplemental information.
- Any additional information required to reanalyze the data reported in this paper is available from the lead contact upon request.

EXPERIMENTAL MODEL AND SUBJECT DETAILS

***In vivo* models—**Two different mouse models that predispose to cachexia were used. A transplanted C26 model of colorectal cancer and the genetically engineered autochthonous KPC model of pancreatic cancer. The C26 model is performed on wild-type BALB/c mice that are inoculated subcutaneously with a syngeneic tumor. In the KPC system, an activating point mutation (G12D) in Kras and a dominant negative mutation in Trp53 (R172H) are conditionally activated in the pancreas by means of the Cre-Lox technology. Both pre-clinical models have been shown to develop tumors that secrete IL-6 and therefore the host is unable to produce ketones during caloric deficiency associated with cachexia, causing a rise in glucocorticoid levels as a consequence. Male KPC were bred in-house, and BALB/c (8 weeks old) mice were obtained from Charles River Laboratories. They were kept in pathogen-free conditions on a 24 hour 12:12 light-dark cycle and allowed to acclimatize for 7 days. All animal experiments and animal care at the MRC CU and CRUK CI were performed in accordance with national and institutional guidelines and approved by the UK Home Office, the animal ethics committee of the University of Cambridge. All animal experiments at CSHL were approved by the Institutional Animal Care and Use Committee (IACUC) and were conducted in accordance with the National Institutes of Health Guide for the Care and Use of Laboratory Animals. Body weights, food intake and clinical signs were monitored on a daily basis. Handling was kept to a minimum. Mice were sacrificed when tumor size exceeded 2 cm length, when weight loss exceeded 15% from peak weight, or when showing clinical signs of discomfort indicative of cachectic endpoint as stated by the Animal Cachexia Score (ACASCO): piloerection, diarrhea or constipation, hunched posture, tremors, and closed eyes [63]. Death was confirmed by cervical dislocation.

Experimental enrolment: Weight-stable, tumor-bearing male KPC mice with tumors of 3–5 mm size and no evidence of obstructive common bile duct, and their respective weight- and age-matched control counterparts (PC mice) were enrolled in the experiments.

Weight-stable wild-type 9-weeks old male BALB/c mice were inoculated with 2×10^6 viable C26 colorectal cancer cells subcutaneously (s.c.) and enrolled on study together with their respective controls.

At day of enrolment (day 14 post-injection of C26 cells), mice were stratified in terms of tumor size, body weight and age, singly-housed and randomly allocated into two experimental matched groups fed with different diets: mice were fed with either standard diet (#5053 PicoLab® Rodent Diet 20; LabDiet) or ketogenic diet (KD) (#F3666; Bio-Serv). Ketogenic diet was given in a Petri dish container that was replaced daily due to potential oxidation of the diet.

Endpoint: Overall survival (OS) or Progression Free Survival (PFS) were the final endpoint of the studies.

Overall Survival: Mice were considered to have reached the OS endpoint when their body weight loss exceeded 15% from their peak weight.

Progression Free Survival: Mice were considered to have reached the PFS endpoint when the volume of their tumors exceeded 2000 mm^3, as measured by handheld calipers.

Dexamethasone treatment: Dexamethasone 21-phosphate disodium salt (#D1159; Sigma-Aldrich) was dissolved in dH_2O and administered intraperitoneally (i.p.) at 1mg/kg daily.

N-acetyl cysteine (NAC) treatment: N-Acetyl-L-cysteine (#A9165; Sigma-Aldrich) was dissolved in 0.9% NaCl sterile saline solution (#Z1377; Thermo Fisher) and administered intraperitoneally (i.p.) at 150mg/kg daily.

Liproxstatin-1 treatment: Liproxstatin-1 (#S7699; Selleck Chemicals) was dissolved in 2% Dimethyl Sulfoxide (DMSO) (#12611S; Cell Signaling), 40% Polyethylene glycol 300 (PEG300) (#S6704; Selleck Chemicals), 2% Tween-80 and 56% double-distilled water (ddH_2O), individually and in this specific order, and administered intraperitoneally (i.p.) at 10mg/kg daily.

RSL3 treatment: RSL3 ((1S,3R)-RSL3) (#HY-100218A; MedChemExpress) was dissolved in 10% DMSO (#12611S; Cell Signaling), 40% PEG300 (#S6704; Selleck Chemicals), 5% Tween-80 and 45% NaCl 0.9% sterile saline solution (#Z1377; Thermo Fisher) and administered intraperitoneally (i.p.) at 5mg/kg daily.

ACTH stimulation test (synacthen test): ACTH (#HOR-279, ProSpec) was reconstituted in dH_20 and injected intraperitoneally at a dose of 1 ug/g body weight. Tail blood was collected at 0-, 15-, 30-, and 60-min intervals for determination of plasma corticosterone levels. Each group consisted of five animals.

Cell lines

C26 murine colorectal cancer cell line: C26 cells were cultured in complete growth medium consisting of RPMI-1640 medium with Glutamine (#11–875-093; Thermo Fisher) containing 10% of Heat-Inactivated Fetal Bovine Serum (FBS) (#10–438-026; Thermo Fisher) and 1x Penicillin-Streptomycin solution (#15–140-122; Thermo Fisher) under sterile conditions. 1x Trypsin-EDTA (#15400054; Thermo Fisher) was used for cell dissociation. Cells were resuspended in FBS-free RPMI and viable cells were counted using a Vi-Cell

counter prior to subcutaneous injection of 2×10^6 viable cells diluted in 100μL RPMI into the right flank of each BALB/c mouse.

H295R human adrenocortical cell line: H295R cells (#CRL-2128; ATCC) were cultured in complete growth medium consisting of DMEM:F12 medium (#30–2006; ATCC) with 0.00625 mg/mL insulin; 0.00625 mg/mL transferrin; 6.25 ng/mL selenium; 1.25 mg/mL bovine serum albumin; 0.00535 mg/mL linoleic acid (ITS+ Premix)(#354352; Corning) and adjusted to a final concentration of 2.5% Nu-Serum I (#355100; Corning). Cells were grown in 75 cm^2 culture flasks and subcultured 1:3 every 3 days. 1x Trypsin-EDTA solution was used for cell dissociation prior to seeding cells in 96-well plates for experimental viability or cortisol release tests.

METHOD DETAILS

Metabolic cages—The Comprehensive Lab Animal Monitoring System (CLAMS) from Columbus Instruments was used to monitor and quantify multiple metabolic parameters such as activity, weight (g), drinking (mL), food intake (g), sleep, and open circuit calorimetry in animal cages that allows precise control over the light/dark cycle. Data from C26-injected or WT BALB/c control mice on standard or ketogenic diet treated with Dexamethasone or vehicle (saline) was collected real-time during an acclimation period (72 hours), a baseline period (72 hours) and during all the experimental timeline (approximately 33 days) through the Oxymax collection software during 10–30 second intervals. Data were collected at 23°C. Data was exported and analyzed in RStudio.

Tumor size—PDAC tumors in KPC mice were detected via palpation and high-resolution ultrasound imaging (Vevo 2100; VisualSonics), and confirmed at necropsy. Tumor growth was monitored by ultrasound scans assessed at multiple angles. Mice were carefully observed for any macroscopic metastases. Maximum cross-sectional area (CSA) and maximum diameter of the tumors were determined for each timepoint. Tumor development in BALB/c mice was spotted via palpation and monitored daily by caliper measurements. Volume of the tumor was calculated as follows: volume (mm^3) = [long axis (mm) x short axis (mm)]^2 / 2.

Blood and plasma measurements—Tail bleeds and terminal cardiac bleeds were always taken at the same time of day (7:30am) and using the same technique. Tail vein bleeds were performed using a scalpel via tail venesection without restraint, and terminal bleeds were obtained through exsanguination via cardiac puncture under isoflurane anesthesia. Tail bleeds were immediately analyzed for glucose and ketone concentration measurements using glucose/ketones stripes and gluco-/keto-meters (Freestyle Optium Neo; Abbott laboratories).

Plasma samples were collected from tail or terminal cardiac bleeds using heparin-coated hematocrit capillary tubes to avoid coagulation and were processed as follows: centrifuge spin at 14,000 rpm for 5 min at 4°C, snap frozen in liquid nitrogen and stored at −80°C.

Corticosterone was quantified from plasma using the International Corticosterone (Human, Rat, Mouse) ELISA (#RE52211; IBL). The sample incubation step from the IBL assay

protocol was 3 hours at room temperature (RT) so as to reach displacement equilibrium as determined by preliminary data. IL-6 levels were measured from plasma using the mouse IL-6 Quantikine ELISA Kit (#M6000B; R&D Systems).

4-hyroxynonenal (4-HNE) measurements in the plasma were quantified using the Universal 4-Hydroxynonenal ELISA Kit (Colorimetric) (#NBP2–66364; Novus Biologicals).

Pregnenolone was measured in the plasma using the Pregnenolone ELISA Kit (Colorimetric) (#NBP2–68102; Novus Biologicals).

Levels of Adrenocorticotropin hormone (ACTH) in the plasma were measured with the Mouse/Rat ACTH ELISA Kit (#ab263880; Abcam).

Tissue collection—Liver, tumor, spleen, adrenal glands, quadricep muscle, lungs, and gonadal and subcutaneous fat samples were collected and weighed during necropsy dissection. Subsequently, tumor, liver and spleen samples were cut into 3 equal parts, which were either snap frozen in liquid nitrogen, cryo-embedded in OCT, or fixed in 4% neutral buffered formaldehyde for 24 hours at room temperature (RT) before either being transferred to 70% ethanol and later paraffin-embedded (FFPE) for immunohistochemistry processing. All the other organs and tissue samples were immediately snap frozen and stored at −80°C.

Tissue lysis—Snap frozen tissues stored at −80°C were transferred to dishes on wet ice and cut into pieces with a scalpel. Each piece was weighed and placed into 2mL round-bottom Eppendorf tubes pre-loaded with Stainless Steel beads (#69989; Qiagen) on wet ice. Homogenizer tubes were then filled up with lysis buffer (#AA-LYS-16ml; RayBiotech) and supplemented with Protease Inhibitor Cocktail (#AA-PI; Raybiotech) and Phosphatase Inhibitor Cocktail Set I (#AA-PHI-I; RayBiotech). Samples were homogenized in Tissue Lyser II (#85300; Qiagen) for 5 minutes and then lysates were centrifuged at 4°C for 20 minutes at maximum speed. The supernatant was harvested and kept on ice if testing fresh or sored at −80°C.

The Bicinchoninic Acid (BCA) Method was used to determine protein concentration in lysates.

Ferrous (Fe^{2+}) and Ferric (Fe^{3+}) iron levels in tissue lysates were measured using the Colorimetric Iron Assay Kit (#ab83366; Abcam).

Quantification of 4-HNE-protein adducts in lysates was performed using the Lipid Peroxidation (4-HNE) Assay Kit (#ab238538; Abcam).

Detection of NADPH levels in the adrenal glands was performed using the NADP/NADPH-Glo™ Bioluminescent Assay (#G9081; Promega).

Oil-Red-O staining—Fresh frozen tissue sections of 5–10 μm thickness were mounted on slides, air dried for 30–60 minutes at RT and fixed in ice cold 10% neutral-buffered formalin (#HT501128–4L; Sigma-Aldrich) for 5–10 minutes. After rinsing in 3 changes of distilled water and air drying for another 30–60 minutes, slides were placed in absolute Propylene

Glycol (#P4347; Sigma-Aldrich) for 2–5 minutes, then stained in pre-warmed Oil Red O solution (#O0625–25G; Sigma-Aldrich) for 8–10 minutes in a 60°C oven, differentiated in 85% Propylene Glycol solution for 2–5 minutes and rinsed in 2 changes of distilled water. Slides were then counterstained with Mayer's hematoxylin (#ab245880; Abcam) for 30 seconds, washed thoroughly with distilled water and mounted with aqueous mounting medium.

Immunohistochemistry—Tissues were fixed in 4% paraformaldehyde (#50–980-495; Thermo Fisher) for 24 h and then embedded in a paraffin wax block. Sectioning with a cryostat, deparaffinization, antigen retrieval and immunohistochemistry for Ki67 (#14–5698-82; Thermo Fisher) was performed by the CRUK CI Histopathology Core using a Leica Bond III autostainer. The slides were scanned on a Leica Aperio AT2 system and subsequently analyzed in a blinded manner. H&E staining was performed by the Histology Facility at Cold Spring Harbor Laboratory. For the staining of 4-HNE adducts in liver tissue, 5μm thick paraffin slides were stained on Discovery Ultra IHC research platform (Roche) following standard protocols. Briefly, after deparaffinization and rehydration, slides were subjected to antigen retrieval (Benchmark Ultra CC1) at 96˚C for 64 minutes; primary Ab incubation with anti-4HNE antibody (#ab48506; Abcam) (1:100) was performed at 37˚C for 1hr and Discovery multimer detection system (Discovery OmniMap HRP, Discovery DAB) was used to detect and amplify immuno-signals.

Metabolomics—Global metabolic profiling of liver and tumor samples was performed by UPLC-MS/MS at Metabolon, Inc. facilities (UK project #CRUK-01–19VW; USA project #CSHL-01–22VW+; results from both datasets were merged). Samples were prepared using the automated MicroLab STAR® system from Hamilton Company. Several recovery standards were added prior to the first step in the extraction process for QC purposes. To remove protein, dissociate small molecules bound to protein or trapped in the precipitated protein matrix, and to recover chemically diverse metabolites, proteins were precipitated with methanol under vigorous shaking for 2 min (Glen Mills GenoGrinder 2000) followed by centrifugation. The resulting extract was divided into five fractions: two for analysis by two separate reverse phases (RP)/UPLC-MS/MS methods with positive ion mode electrospray ionization (ESI), one for analysis by RP/UPLC-MS/MS with negative ion mode ESI, one for analysis by HILIC/UPLC-MS/MS with negative ion mode ESI, and one sample was reserved for backup. Samples were placed briefly on a TurboVap® (Zymark) to remove the organic solvent. The sample extracts were stored overnight under nitrogen before preparation for analysis.

Raw data were extracted, peak-identified and QC processed using Metabolon's hardware and software. These systems are built on a web-service platform utilizing Microsoft's .NET technologies, which run on high-performance application servers and fiber-channel storage arrays in clusters to provide active failover and load-balancing. Compounds were identified by comparison to library entries of purified standards or recurrent unknown entities. Metabolon maintains a library based on authenticated standards that contains the retention time/index (RI), mass to charge ratio (m/z), and chromatographic data (including MS/MS spectral data) on all molecules present in the library. Furthermore, biochemical

identifications are based on three criteria: retention index within a narrow RI window of the proposed identification, accurate mass match to the library +/− 10 ppm, and the MS/MS forward and reverse scores between the experimental data and authentic standards.

A total of 685 and 669 named metabolites were retained for liver and tumor datasets, respectively. Following log transformation and imputation of missing values, if any, with the minimum observed value for each compound, Welch's two-sample t-test was used to identify biochemicals that differed significantly between experimental groups. An estimate of the false discovery rate (q-value) was calculated to take into account the multiple comparisons that normally occur in metabolomic-based studies.

H295R Cortisol synthesis assay—H295R cells were seeded in 96-well plates with 12,000 cells in 200 μL of complete growth medium for each well and allowed to settle for 48 hours. The medium was then changed and 200 μL medium containing specific LPPs was added. LPPs used: 4-hydroxynonenal (4-HNE) (#32100; Cayman Chemical), 4-hydroxyhexenal (4-HHE) (#32060; Cayman Chemical) and malondialdehyde (MDA) (#63287–1G-F; Sigma-Aldrich). After 48 or 72 hours of incubation in the presence of the compound, the medium was carefully collected, transferred to the test tubes and immediately stored at −20°C. Cells in each well were detached and counted by Trypan Blue staining (#15250061; Thermo Fisher). Samples were diluted 1:5 and cortisol levels were measured using a Cortisol Competitive Human ELISA Kit (#EIAHCOR; Thermo Fisher) according to the manufacturer's protocol.

Sulforhodamine B (SRB) colorimetric assay—A total of 12,000 cells per well were seeded in a 96-wells plate. Two days after seeding, media was replaced and cells were treated with increasing concentrations of a specific LPP for 72h. Then, cells were fixed with 1% trichloroacetic acid (#T9159–100G; Sigma-Aldrich) at 4 °C for 30 min, washed 3 times with distilled water and stained with 0.057% SRB (#S1402–5G; Sigma-Aldrich) in 1% acetic acid (#A6283, Sigma-Aldrich) solution at RT for 30 min. Following staining, cells were washed 3 times with 1% acetic acid and air-dried overnight. The protein bound dye was dissolved in 10 mM Tris base solution and the absorbance was measured at 565 nm using a microplate reader (SpectraMax i3x).

Single cell preparation—Cell suspensions were prepared from tissues by mechanical dissociation, followed by digestion in 5 mL of RPMI-1640 containing collagenase I (500 U/mL) (#SCR103; Sigma-Aldrich) and DNase I (0.2 mg/mL) (#04716728001; Sigma-Aldrich) for 45 min at 37°C on a shaker (220 rpm), followed by filtration through a 70-μm strainer and 25% Percoll (#GE17–0891-01; Sigma-Aldrich) gradient enrichment of leukocytes, and red blood cell (RBC) lysis. Tumor cells were recovered without Percoll enrichment. Blood cells were lysed in 5 mL of RBC lysis buffer (#A1049201; Thermo Fisher) three times for 5 min, and spleens were strained through a 70-μm filter in RPMI-1640 before lysing erythrocytes with RBC lysis buffer for 5 min. Single cells were restimulated and stained for surface and intracellular markers (see flow cytometry below).

Flow cytometry—Cell sorting was performed using a FACSAria™ Cell Sorter (BD Biosciences) at CSHL Flow Cytometry Facility. FlowJo X (Tree Star) software was used for experimental analysis.

The following antibodies were used: Alexa Fluor 700 anti-mouse CD45 (#103127; BioLegend), FITC anti-mouse CD45 (#11–0451; Thermo Fisher), APC/Cy7 anti-mouse CD3ε (#100329; BioLegend), PerCP/Cyanine 5.5 anti-mouse CD4 (#100433; BioLegend), Brilliant Violet 510TM anti-mouse CD8a (#100751; BioLegend), Brilliant Violet 605TM anti-mouse/human CD11b (#101257; BioLegend), Alexa Fluor 700 anti-mouse Ly-6G/Ly-6C (Gr-1) (#108421; BioLegend), FITC anti-mouse CD69 (#104505; BioLegend), PE/Cy7 anti-mouse CD152 (#106313; BioLegend); Brilliant Violet 421TM anti-mouse CD274 (#124315; BioLegend), PE/Dazzle 594 anti-mouse CD279 (#109115; BioLegnd), and FITC anti-mouse F4/80 (#123107; BioLegend).

Western blotting—Cells were lysed in RIPA buffer (50mM Tris HCl, pH 7.4, 150mM NaCl, 0.5% deoxycholate, 0.1% sodium dodecyl sulphate, 1% NP-40) (#89901; Thermo Fisher) containing protease inhibitors (#78442; Thermo Fisher) and 1 mM dithiothreitol (DTT) (#A39255; Thermo Fisher). Whole cell extracts were separated by electrophoresis, transferred onto nitrocellulose membranes (#88025; Thermo Fisher) and blocked in 5% non-fat dry milk (#1706404; Bio-Rad) dissolved in 0.1% Tween/TBS. Membranes were incubated with primary antibodies: BAX Rabbit mAb (#50599–2-Ig; Proteintech, 1:500), β-Actin Rabbit mAb (#4967; Cell Signaling Technology, 1:5000) and Caspase-3 (D3R6Y) Rabbit mAb (#14220; Cell Signaling, 1:1000), overnight at 4°C followed by washing in 0.1% Tween/TBS. Membranes were incubated with Goat Anti-Rabbit IgG H&L (HRP) secondary antibodies (#ab205718; Abcam, 1:5000) at 25°C for 1h and washed thrice prior to signal detection. Membranes were developed by exposure in a dark room through chemiluminescence using ECL reagent (#32106; Thermo Fisher).

qRT-PCR—mRNA was extracted from frozen tissues using QIAzol Lysis Reagent (#79306; Qiagen) and the Tissue Lyser II (#85300; Qiagen), following the manufacture's protocol for the RNeasy Lipid Tissue Mini Kit (#74804, Qiagen) in an automated manner with the QIAcube Connect (#9002864; Qiagen). Concentration and purity of aqueous RNA was assessed using a NanoDrop™ Spectrophotometer (#ND-ONE-W; Thermo Fisher). mRNA templates from muscle and liver samples were diluted to 2ng/μl and mRNA was analysed by quantitative Real-Time PCR using the TaqMan™ RNA-to-CT™ 1-Step Kit (#4392653; Thermo Fisher). mRNA levels were normalized to either Rn18s (liver) or Tbp (quadriceps) using the ddCt method. The following TaqMan primers were used: Mm01277044_m1 (Tbp); Mm03928990_g1 (Rn18s); Mm00440939_m1 (Ppara); Mm01323360_g1 (Acadm); Mm00550050_m1 (Hmgcs2); Mm00499523_m1 (Fbxo32); and Mm01185221_m1 (Trim63).

RNA-sequencing—RNA extracted from frozen tissues via QIAzol Lysis Reagent (#79306; Qiagen) was run through RNeasy spin columns following the RNeasy Lipid Tissue Mini Kit in an automated manner with the QIAcube Connect (#9002864; Qiagen). Integrity was confirmed using RIN values with a cut-off of 8. Libraries were prepared by the Next Gen Sequencing Core at CSHL using the Illumina TruSeq mRNA Stranded Sample prep kit

(96 index High Throughput) and normalized using Kapa Biosystem's Library Quantification Kit. NextSeq High Output Paired-End 150bp was run for sequencing.

For the analysis, reads were aligned to the mouse genome version GRCm38.74 and read counts were obtained using "biomaRt" R package. "org.Mm.eg.db" R package was used for genome wide annotation. Read counts were normalized and tested for differential gene expression using the Bioconductor package "edgeR". Multiple testing correction was applied using the Benjamini-Hochberg procedure (FDR <0.05). "fgsea" and "dplyr" packages were used for GSEA in R. GSEA was performed by ranking all genes tested in RNA-Seq using –log10 (p-values) derived from differential expression analyses and testing against MSigDB Hallmark gene sets and Canonical pathways KEGG gene sets. Results were curated using a p-adj <0.05 threshold.

QUANTIFICATION AND STATISTICAL ANALYSIS

Data were expressed as the mean ± SEM unless otherwise stated. Statistical analyses were performed using GraphPad Prism 7.03 software or RStudio software. Normality of data distribution was tested with the Shapiro-Wilk test. The log-rank (Mantel–Cox) test was used to compare survival distributions. Two-tailed Student's t-test were used to compare two groups. When comparing 3 or more groups, one-way ANOVA with Tukey's correction for post-hoc testing was used. For statistical comparison of quantitative data at different times, unpaired two-tailed Student's t-tests were performed at each timepoint with the Holm-Sidak method correction for multiple comparisons. To analyze multiple parameters, such as the main independent effect of diet and cancer and the interaction of both factors, two-way ANOVA tests were used. All cell-based in vitro experiments were independently repeated three times in triplicate. For global metabolic profiling of liver and tumor, a Principal Component Analysis (PCA) was performed. Differences in tumor growth were assessed by fitting a mixed effect model with coefficients for the intercept, slope and the difference in the slope between diets, and a random component for each individual mouse. Significance was assessed by testing whether the coefficient for the difference in the slope was significantly different from zero using a t-test. One-way ANCOVA was conducted to determine statistical significances in on total energy expenditure (TEE) controlling for weight. P-values and sample size can be found in main and supplementary figure legends.

Supplementary Material

Refer to Web version on PubMed Central for supplementary material.

ACKNOWLEDGMENTS

Miriam Ferrer is supported by the "la Caixa" Foundation (ID 100010434) in the framework of the "La Caixa" Fellowship Program under agreement LCF/BQ/AA18/11680037, and by the MRC Cancer Unit with a Doctoral Training Award. Tobias Janowitz acknowledges funding from Cancer Grand Challenges (NIH: 1OT2CA278690-01; CRUK: CGCATF-2021/100019), Cancer Research UK (C42738/A24868), The Mark Foundation for Cancer Research (33300111), Cold Spring Harbor Laboratory (CSHL), and developmental funds from CSHL Cancer Center Support Grant 5P30CA045508. The CRUK CI (Li Ka Shing Centre) where some of this work was performed was generously funded by CK Hutchison Holdings Limited, the University of Cambridge, CRUK, The Atlantic Philanthropies and others. We thank the Preclinical Genome Editing Core (TMC sub team) at CRUK CI and the Core Facilities at CSHL for assistance. This work was supported by Medical Research Council (MRC) Programme grants MC_UU_12022/1 and MC_UU_12022/8 to Ashok R. Venkitaraman.

REFERENCES

1. Warburg O. (1925). The metabolism of carcinoma cells 1. J. Cancer Res. 9, 148–163. 10.1158/jcr.1925.148.
2. von Haehling S, and Anker SD (2014). Prevalence, incidence and clinical impact of cachexia: facts and numbers—update 2014. J. Cachexia. Sarcopenia Muscle 5, 261–263. 10.1007/s13539-014-0164-8. [PubMed: 25384990]
3. Farkas J, von Haehling S, Kalantar-Zadeh K, Morley JE, Anker SD, and Lainscak M. (2013). Cachexia as a major public health problem: Frequent, costly, and deadly. J. Cachexia. Sarcopenia Muscle 4, 173–178. 10.1007/s13539-013-0105-y. [PubMed: 23539127]
4. Jansen N, and Walach H. (2016). The development of tumours under a ketogenic diet in association with the novel tumour marker TKTL1: A case series in general practice. Oncol. Lett. 11, 584–592. 10.3892/ol.2015.3923. [PubMed: 26870251]
5. Otto C, Kaemmerer U, Illert B, Muehling B, Pfetzer N, Wittig R, Voelker HU, Thiede A, and Coy JF (2008). Growth of human gastric cancer cells in nude mice is delayed by a ketogenic diet supplemented with omega-3 fatty acids and medium-chain triglycerides. BMC Cancer 8, 1–12. 10.1186/1471-2407-8-122. [PubMed: 18173856]
6. Nakamura K, Tonouchi H, Sasayama A, and Ashida K. (2018). A ketogenic formula prevents tumor progression and cancer cachexia by attenuating systemic inflammation in colon 26 tumor-bearing mice. Nutrients 10. 10.3390/nu10020206.
7. Seyfried TN, Sanderson TM, El-Abbadi MM, McGowan R, and Mukherjee P. (2003). Role of glucose and ketone bodies in the metabolic control of experimental brain cancer. Br. J. Cancer 89, 1375–1382. 10.1038/sj.bjc.6601269. [PubMed: 14520474]
8. Schwartz K, Chang HT, Nikolai M, Pernicone J, Rhee S, Olson K, Kurniali PC, Hord NG, and Noel M. (2015). Treatment of glioma patients with ketogenic diets: report of two cases treated with an IRB-approved energy-restricted ketogenic diet protocol and review of the literature. Cancer Metab. 3, 1–10. 10.1186/s40170-015-0129-1. [PubMed: 25621173]
9. Flint TR, Janowitz T, Connell CM, Roberts EW, Denton AE, Coll AP, Jodrell DI, and Fearon DT (2016). Tumor-Induced IL-6 Reprograms Host Metabolism to Suppress Anti-tumor Immunity. Cell Metab. 24, 672–684. 10.1016/j.cmet.2016.10.010. [PubMed: 27829137]
10. Goncalves MD, Hwang SK, Pauli C, Murphy CJ, Cheng Z, Hopkins BD, Wu D, Loughran RM, Emerling BM, Zhang G, et al. (2018). Fenofibrate prevents skeletal muscle loss in mice with lung cancer. Proc. Natl. Acad. Sci. U. S. A. 115, E743–E752. 10.1073/pnas.1714703115. [PubMed: 29311302]
11. Massey KA, and Nicolaou A. (2011). Lipidomics of polyunsaturated-fatty-acid-derived oxygenated metabolites. Biochem. Soc. Trans. 39, 1240–1246. 10.1042/BST0391240. [PubMed: 21936796]
12. Yin H, Xu L, and Porter NA (2011). Free radical lipid peroxidation: Mechanisms and analysis. Chem. Rev. 111, 5944–5972. 10.1021/cr200084z. [PubMed: 21861450]
13. Nair J, Vaca CE, Velic I, Mutanen M, Valsta LM, and Bartsch H. (2019). High dietary w-6 Polyunsaturated Fatty Acids Drastically Increase the Formation of Etheno-DNA Base Adducts in White Blood Cells of Female Subjects. J. Chem. Inf. Model. 53, 1689–1699. 10.1017/CBO9781107415324.004.
14. Goldstein BD (1975). Mutagenicity of Malonaldehyde, a Decomposition Product of Peroxidized Polyunsaturated Fatty Acids. Science (80-.). 191.
15. Little C, and O'Brien PJ (1968). An intracellular GSH-peroxidase with a lipid peroxide substrate. Biochem. Biophys. Res. Commun. 31, 145–150. 10.1016/0006-291X(68)90721-3. [PubMed: 5656060]
16. Ursini F, Maiorino M, Valente M, Ferri L, and Gregolin C. (1982). Purification from pig liver of a protein which protects liposomes and biomembranes from peroxidative degradation and exhibits glutathione peroxidase activity on phosphatidylcholine hydroperoxides. Biochim. Biophys. Acta (BBA)/Lipids Lipid Metab. 710, 197–211. 10.1016/0005-2760(82)90150-3.
17. Yang WS, Sriramaratnam R, Welsch ME, Shimada K, Skouta R, Viswanathan VS, Cheah JH, Clemons PA, Shamji F, Clish CB, et al. (2014). Regulation of Ferroptotic Cancer Cell Death by GPX4. Cell 156, 317–331. 10.1016/j.cell.2013.12.010.Regulation. [PubMed: 24439385]

18. Hoberman HD (1950). Endocrine regulation of amino acid protein metabolism during fasting. Yale J. Biol. Med. 22, 341–367. [PubMed: 15410433]
19. Wing SS, and Goldberg AL (1993). Glucocorticoids activate the ATP-ubiquitin-dependent proteolytic system in skeletal muscle during fasting. Am. J. Physiol. - Endocrinol. Metab. 264. 10.1152/ajpendo.1993.264.4.e668.
20. Divertie GD, Jensen MD, and Miles JM (1991). Stimulation of Lipolysis in Humans by Physiological Hypercortisolemia. 40.
21. Bratland E, Skinningsrud B, Undlien DE, Mozes E, and Husebye ES (2009). T cell responses to steroid cytochrome P450 21-hydroxylase in patients with autoimmune primary adrenal insufficiency. J. Clin. Endocrinol. Metab. 94, 5117–5124. 10.1210/jc.2009-1115. [PubMed: 19890026]
22. Henzen C, Suter A, Lerch E, Urbinelli R, Schorno XH, and Briner VA (2000). Suppression and recovery of adrenal response after short-term, high-dose glucocorticoid treatment. Lancet 355, 542–545. 10.1016/S0140-6736(99)06290-X. [PubMed: 10683005]
23. Dello SAWG, Neis EPJG, de Jong MC, van Eijk HMH, Kicken CH, Olde Damink SWM, and Dejong CHC (2013). Systematic review of ophthalmate as a novel biomarker of hepatic glutathione depletion. Clin. Nutr. 32, 325–330. 10.1016/j.clnu.2012.10.008. [PubMed: 23182341]
24. Scuto M, Salinaro AT, Modafferi S, Polimeni A, Pfeffer T, Weigand T, Calabrese V, Schmitt CP, and Peters V. (2020). Carnosine activates cellular stress response in podocytes and reduces glycative and lipoperoxidative stress. Biomedicines 8, 1–14. 10.3390/BIOMEDICINES8060177.
25. Fontana M, Amendola D, Orsini E, Boffi A, and Pecci L. (2005). Oxidation of hypotaurine and cysteine sulphinic acid by peroxynitrite. Biochem. J. 389, 233–240. 10.1042/BJ20041696. [PubMed: 15740460]
26. Dixon SJ, Lemberg KM, Lamprecht MR, Skouta R, Zaitsev EM, Gleason CE, Patel DN, Bauer AJ, Cantley AM, Yang WS, et al. (2012). Ferroptosis: An Iron-Dependent Form of Non-Apoptotic Cell Death. Cell 149, 1060–1072. 10.1016/j.cell.2012.03.042.Ferroptosis. [PubMed: 22632970]
27. Badgley MA, Kremer DM, Carlo Maurer H, DelGiorno KE, Lee HJ, Purohit V, Sagalovskiy IR, Ma A, Kapilian J, Firl CEM, et al. (2020). Cysteine depletion induces pancreatic tumor ferroptosis in mice. Science (80-.). 368, 85–89. 10.1126/science.aaw9872.
28. Zhang B, Chen X, Ru F, Gan Y, Li B, Xia W, Dai G, He Y, and Chen Z. (2021). Liproxstatin-1 attenuates unilateral ureteral obstruction-induced renal fibrosis by inhibiting renal tubular epithelial cells ferroptosis. Cell Death Dis. 12, 1–10. 10.1038/s41419-021-04137-1. [PubMed: 33414393]
29. Yang J, Mo J, Dai J, Ye C, Cen W, Zheng X, Jiang L, and Ye L. (2021). Cetuximab promotes RSL3-induced ferroptosis by suppressing the Nrf2/HO-1 signalling pathway in KRAS mutant colorectal cancer. Cell Death Dis. 12, 1–11. 10.1038/s41419-021-04367-3. [PubMed: 33414393]
30. Dong Y, Tu R, Liu H, and Qing G. (2020). Regulation of cancer cell metabolism: oncogenic MYC in the driver's seat. Signal Transduct. Target. Ther. 5. 10.1038/s41392-020-00235-2.
31. Mishima E. (2021). The E2F1-IREB2 axis regulates neuronal ferroptosis in cerebral ischemia. Hypertens. Res, 1085–1086. 10.1038/s41440-021-00837-5. [PubMed: 34952951]
32. Lu Y, Yang Q, Su Y, Ji Y, Li G, Yang X, Xu L, Lu Z, Dong J, Wu Y, et al. (2021). MYCN mediates TFRC-dependent ferroptosis and reveals vulnerabilities in neuroblastoma. Cell Death Dis. 12. 10.1038/s41419-021-03790-w.
33. Alborzinia H, Flórez AF, Kreth S, Brückner LM, Yildiz U, Gartlgruber M, Odoni DI, Poschet G, Garbowicz K, Shao C, et al. (2022). MYCN mediates cysteine addiction and sensitizes neuroblastoma to ferroptosis. Nat. Cancer 3, 471–485. 10.1038/s43018-022-00355-4. [PubMed: 35484422]
34. Efimova I, Catanzaro E, Van Der Meeren L, Turubanova VD, Hammad H, Mishchenko TA, Vedunova MV, Fimognari C, Bachert C, Coppieters F, et al. (2020). Vaccination with early ferroptotic cancer cells induces efficient antitumor immunity. J. Immunother. Cancer 8, 1–15. 10.1136/jitc-2020-001369.
35. Bethin KE, Vogt SK, and Muglia LJ (2000). Interleukin-6 is an essential, corticotropin-releasing hormone-independent stimulator of the adrenal axis during immune system activation. Proc. Natl. Acad. Sci. U. S. A. 97, 9317–9322. 10.1073/pnas.97.16.9317. [PubMed: 10922080]

36. Žarković M, Ignjatović S, Dajak M, Ćirić J, Beleslin B, Savić S, Stojković M, Bulat P, and Trbojević B. (2008). Cortisol response to ACTH stimulation correlates with blood interleukin 6 concentration in healthy humans. Eur. J. Endocrinol. 159, 649–652. 10.1530/EJE-08-0544. [PubMed: 18753312]
37. Salas MA, Evans SW, Levell MJ, and Whicher JT (1990). Interleukin-6 and ACTH act synergistically to stimulate the release of corticosterone from adrenal gland cells. Clin. Exp. Immunol. 79, 470–473. 10.1111/j.1365-2249.1990.tb08114.x. [PubMed: 2156641]
38. Mol M, Regazzoni L, Altomare A, Degani G, Carini M, Vistoli G, and Aldini G. (2017). Enzymatic and non-enzymatic detoxification of 4-hydroxynonenal: Methodological aspects and biological consequences. Free Radic. Biol. Med. 111, 328–344. 10.1016/j.freeradbiomed.2017.01.036. [PubMed: 28161307]
39. Patel S, Alvarez-Guaita A, Melvin A, Rimmington D, Dattilo A, Miedzybrodzka EL, Cimino I, Maurin AC, Roberts GP, Meek CL, et al. (2019). GDF15 Provides an Endocrine Signal of Nutritional Stress in Mice and Humans. Cell Metab. 29, 707–718.e8. 10.1016/j.cmet.2018.12.016. [PubMed: 30639358]
40. Hsu JY, Crawley S, Chen M, Ayupova DA, Lindhout DA, Higbee J, Kutach A, Joo W, Gao Z, Fu D, et al. (2017). Non-homeostatic body weight regulation through a brainstem-restricted receptor for GDF15. Nature 550, 255–259. 10.1038/nature24042. [PubMed: 28953886]
41. Mulderrig L, Garaycoechea JI, Tuong ZK, Millington CL, Dingler FA, Ferdinand JR, Gaul L, Tadross JA, Arends MJ, O'Rahilly S, et al. (2021). Aldehyde-driven transcriptional stress triggers an anorexic DNA damage response. Nature 600, 158–163. 10.1038/s41586-021-04133-7. [PubMed: 34819667]
42. Yuan L, Han J, Meng Q, Xi Q, Zhuang Q, Jiang Y, Han Y, Zhang B, Fang J, and Wu G. (2015). Muscle-specific E3 ubiquitin ligases are involved in muscle atrophy of cancer cachexia: An in vitro and in vivo study. Oncol. Rep. 33, 2261–2268. 10.3892/or.2015.3845. [PubMed: 25760630]
43. Corbello Pereira SR, Darronqui E, Constantin J, Alves Da Silva MHDR, Yamamoto NS, and Bracht A. (2004). The urea cycle and related pathways in the liver of Walker-256 tumor-bearing rats. Biochim. Biophys. Acta - Mol. Basis Dis. 1688, 187–196. 10.1016/j.bbadis.2003.12.001.
44. Haines RW, Zolfaghari P, Wan Y, Pearse RM, Puthucheary Z, and Prowle JR (2019). Elevated urea-to-creatinine ratio provides a biochemical signature of muscle catabolism and persistent critical illness after major trauma. Intensive Care Med. 45, 1718–1731. 10.1007/s00134-019-05760-5. [PubMed: 31531715]
45. Anderson NM, Mucka P, Kern JG, and Feng H. (2018). The emerging role and targetability of the TCA cycle in cancer metabolism. Protein Cell 9, 216–237. 10.1007/s13238-017-0451-1. [PubMed: 28748451]
46. Rui L. (2014). Energy Metabolism in the Liver. Compr Physiol. 4, 177–197. 10.1002/cphy.c130024.Energy. [PubMed: 24692138]
47. Mager DE, Lin SX, Blum RA, Lates CD, and Jusko WJ (2003). Dose Equivalency Evaluation of Major Corticosteroids: Pharmacokinetics and Cell Trafficking and Cortisol Dynamics. J. Clin. Pharmacol. 43, 1216–1227. 10.1177/0091270003258651. [PubMed: 14551176]
48. Liu D, Ahmet A, Ward L, Krishnamoorthy P, Mandelcorn ED, Leigh R, Brown JP, Cohen A, and Kim H. (2013). A practical guide to the monitoring and management of the complications of systemic corticosteroid therapy. Allergy, Asthma Clin. Immunol. 9, 1–25. 10.1186/1710-1492-9-30. [PubMed: 23305328]
49. Bhandarkar NS, Lahav R, Maixner N, Haim Y, Wong GW, Rudich A, and Yoel U. (2021). Adaptation of fuel selection to acute decrease in voluntary energy expenditure is governed by dietary macronutrient composition in mice. Physiol. Rep. 9, 1–8. 10.14814/phy2.15044.
50. Fernández-Verdejo R, Ravussin E, Speakman JR, and Galgani JE (2019). Progress and challenges in analyzing rodent energy expenditure. Nat. Methods 16, 797–799. 10.1038/s41592-019-0513-9. [PubMed: 31391589]
51. Hursting SD, and Berger NA (2010). Energy balance, host-related factors, and cancer progression. J. Clin. Oncol. 28, 4058–4065. 10.1200/JCO.2010.27.9935. [PubMed: 20697088]
52. Janowitz T. (2018). Cancer: The Tumor-Driven Disease of the Host. Cell Metab. 28, 5–6. 10.1016/j.cmet.2018.06.016. [PubMed: 29972797]

53. Fucà G, Galli G, Poggi M, Lo Russo G, Proto C, Imbimbo M, Ferrara R, Zilembo N, Ganzinelli M, Sica A, et al. (2019). Modulation of peripheral blood immune cells by early use of steroids and its association with clinical outcomes in patients with metastatic non-small cell lung cancer treated with immune checkpoint inhibitors. ESMO Open 4, 1–8. 10.1136/esmoopen-2018-000457.
54. Arbour KC, Mezquita L, Long N, Rizvi H, Auclin E, Ni A, Martínez-Bernal G, Ferrara R, Victoria Lai W, Hendriks LEL, et al. (2018). Impact of baseline steroids on efficacy of programmed cell death-1 and programmed death-ligand 1 blockade in patients with non–small-cell lung cancer. J. Clin. Oncol. 36, 2872–2878. 10.1200/JCO.2018.79.0006. [PubMed: 30125216]
55. Eggermont AMM, Kicinski M, Blank CU, Mandala M, Long GV, Atkinson V, Dalle S, Haydon A, Khattak A, Carlino MS, et al. (2020). Association between Immune-Related Adverse Events and Recurrence-Free Survival among Patients with Stage III Melanoma Randomized to Receive Pembrolizumab or Placebo: A Secondary Analysis of a Randomized Clinical Trial. JAMA Oncol. 6, 519–527. 10.1001/jamaoncol.2019.5570. [PubMed: 31895407]
56. Massucci M, Di Fabio F, Rojas Llimpe FL, and Ardizzoni A. (2020). A Case of Response to Immunotherapy in a Patient with MSI Metastatic Colorectal Cancer and Autoimmune Disease in Steroid Therapy. J. Immunother. 43, 153–155. 10.1097/CJI.0000000000000308. [PubMed: 31913208]
57. Menzies AM, Johnson DB, Ramanujam S, Atkinson VG, Wong ANM, Park JJ, McQuade JL, Shoushtari AN, Tsai KK, Eroglu Z, et al. (2017). Anti-PD-1 therapy in patients with advanced melanoma and preexisting autoimmune disorders or major toxicity with ipilimumab. Ann. Oncol. 28, 368–376. 10.1093/annonc/mdw443. [PubMed: 27687304]
58. Hopkins BD, Pauli C, Xing D, Wang DG, Li X, Wu D, Amadiume SC, Goncalves MD, Hodakoski C, Lundquist MR, et al. (2018). Suppression of insulin feedback enhances the efficacy of PI3K inhibitors. Nature 560, 499–503. 10.1038/s41586-018-0343-4. [PubMed: 30051890]
59. Maddocks ODK, Athineos D, Cheung EC, Lee P, Zhang T, Van Den Broek NJF, Mackay GM, Labuschagne CF, Gay D, Kruiswijk F, et al. (2017). Modulating the therapeutic response of tumours to dietary serine and glycine starvation. Nature 544, 372–376. 10.1038/nature22056. [PubMed: 28425994]
60. de Groot S, Lugtenberg RT, Cohen D, Welters MJP, Ehsan I, Vreeswijk MPG, Smit VTHBM, de Graaf H, Heijns JB, Portielje JEA, et al. (2020). Fasting mimicking diet as an adjunct to neoadjuvant chemotherapy for breast cancer in the multicentre randomized phase 2 DIRECT trial. Nat. Commun. 11, 1–9. 10.1038/s41467-020-16138-3. [PubMed: 31911652]
61. Pissios P, Hong S, Kennedy AR, Prasad D, Liu FF, and Maratos-Flier E. (2013). Methionine and choline regulate the metabolic phenotype of a ketogenic diet. Mol. Metab. 2, 306–313. 10.1016/j.molmet.2013.07.003. [PubMed: 24049742]
62. Lien EC, Westermark AM, Zhang Y, Yuan C, Li Z, Lau AN, Sapp KM, Wolpin BM, and Vander Heiden MG (2021). Low glycaemic diets alter lipid metabolism to influence tumour growth. Nature 599, 302–307. 10.1038/s41586-021-04049-2. [PubMed: 34671163]
63. Betancourt A, Busquets S, Ponce M, Toledo M, Guàrdia-Olmos J, Peró-Cebollero M, López-Soriano FJ, and Argilés JM (2019). The animal cachexia score (ACASCO). Anim. Model. Exp. Med. 2, 201–209. 10.1002/ame2.12082.

HIGHLIGHTS

- Ketogenic diet delays tumor growth but accelerates cancer cachexia and shortens survival
- In the tumor, accumulation of lipid peroxidation products results in saturation of the GSH detoxifying pathway and ferroptotic death of cancer cells
- In the host organism, systemic redox state imbalance causes NADPH depletion, GDF-15 elevations, and relative corticosterone deficiency
- Dexamethasone coadministration with ketogenic diet delays onset of cancer cachexia by improving food intake, glucose levels and utilization of nutritional substrates, and has no impact on delayed tumor growth

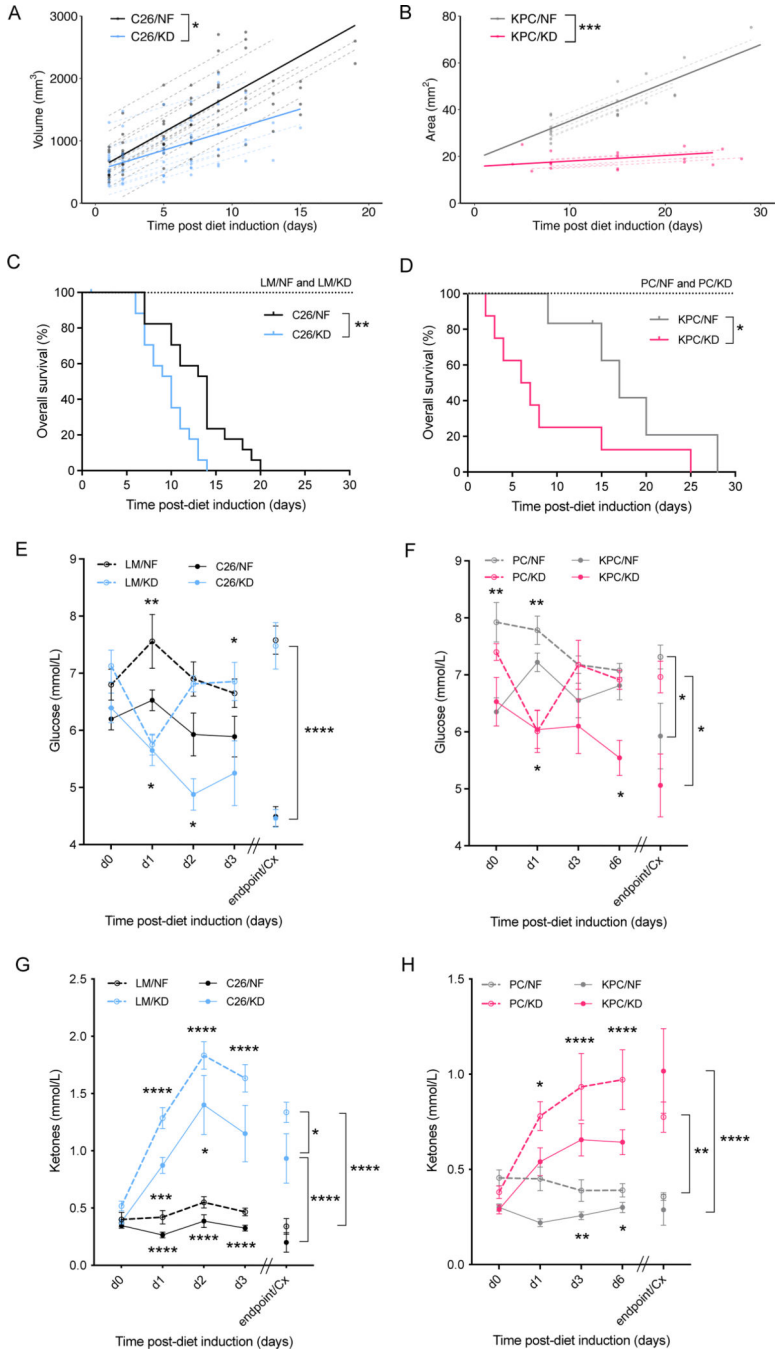

Figure 1. KD delays tumor growth but shortens OS in C26 and KPC murine models of cancer cachexia.

(A) Longitudinal tumor volume in C26 mice fed KD or NF (n=12). (B) Longitudinal tumor area in KPC mice fed KD or NF (n=8). (C) OS of C26 and LM mice on KD or NF (n=7 LM, n=17 C26). (D) OS of KPC and PC mice fed KD or NF (n=5–8). (E-F) Longitudinal glucose measurements in C26 and LM mice (n=7–14 LM, n=20 C26) I, and in KPC and PC mice (n=8–10) (F), fed either KD or NF. (G-H) Longitudinal ketone measurements in C26 and LM mice (n=5–14 LM, n=22–23 C26) (G), and in KPC and PC mice (n=8–10) (H), fed either KD or NF.

Overall survival (OS): time until mice reach >15% bodyweight loss. Differences in (A-B) were assessed by fitting a mixed effect model with a random component for each individual mouse. Kaplan–Meier curves in (C-D) were statistically analyzed by using the log-rank (Mantel–Cox) test. Two-way ANOVA statistical tests with Tukey's correction for post hoc comparisons were performed in (E-H).

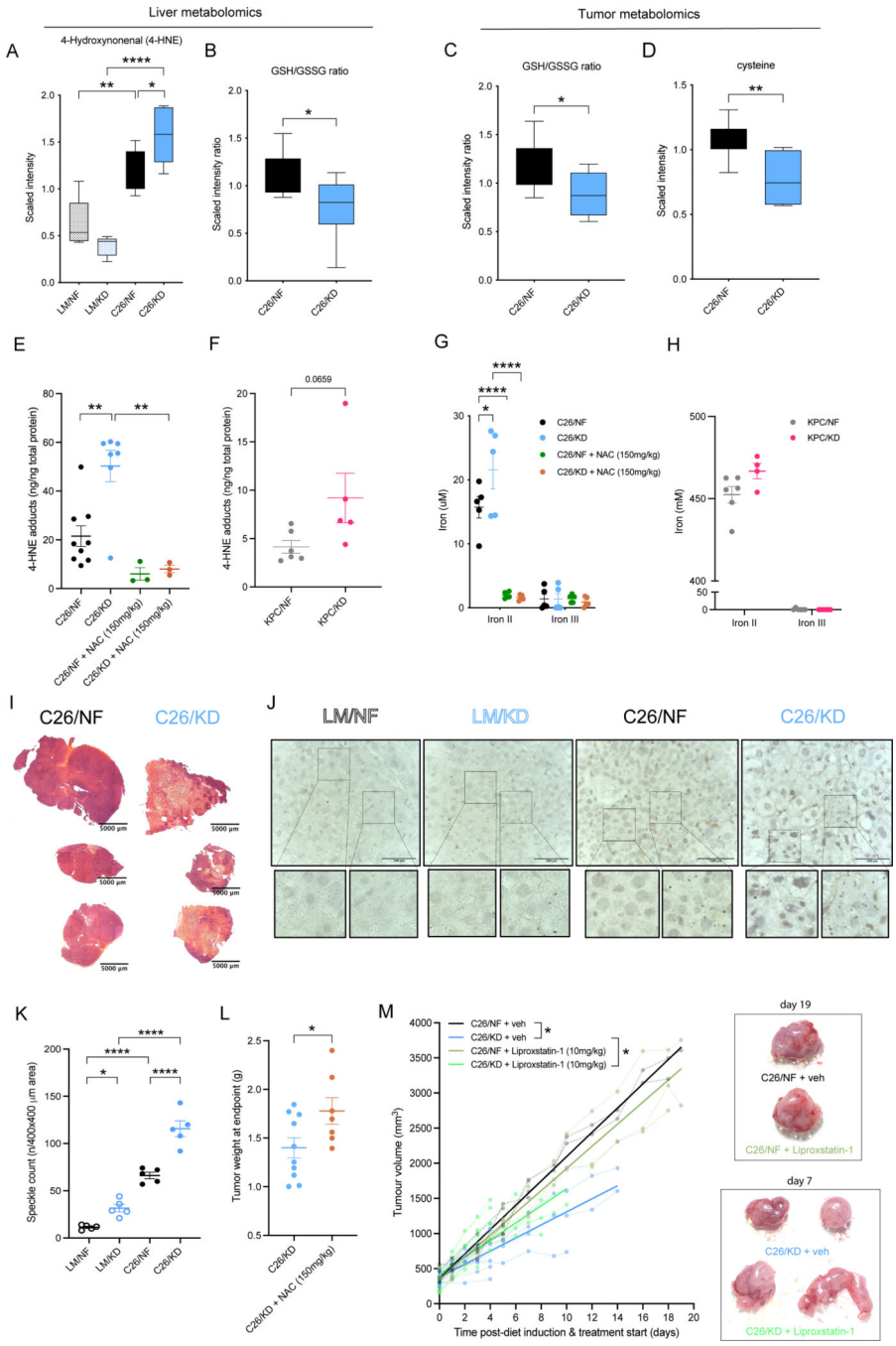

Figure 2. KD induces ferroptotic cell death of cancer cells that can be prevented by NAC.

(A-B) Quantification by UPLC-MS/MS of 4-HNE (A) and GSH/GSSG ratio (B) in the liver of C26 and LM mice on KD or NF (n=5–8). (C-D) Quantification by UPLC-MS/MS of GSH/GSSG ratio (C) and cysteine (D) in the tumor of C26 mice (n=7). (E-F) Detection of 4-HNE adducts in tumor lysates from C26 mice untreated or treated with NAC (n=3) © and from KPC mice (n=5–6) (F) fed KD or NF. (G-H) Iron concentration in tumors from C26 mice fed KD or NF, untreated or treated with NAC (n=5) (G), and in tumors from KPC mice fed KD or NF (n=6) (H). (I) H&E staining of tumors from C26 mice fed KD or NF. (J-K)

Representative images of IHC staining (J) and quantification of speckle pattern formation (K) in liver tissue from C26 and LM mice fed KD or NF. (L) Tumor weight at the time of cachexia in C26 mice fed KD untreated or treated with NAC (n=7–10). (M) Longitudinal tumor growth in C26 mice fed KD or NF, and treated with Liproxstatin-1 (10mg/kg) or vehicle (n=5–10).

One-way ANOVA with Tukey's correction for post hoc testing was used in (A, E, G, K). Statistical differences in (B-D, H, L) were examined using an unpaired two-tailed Student's t-test with Welch's correction. Simple linear regression model was applied to (M).

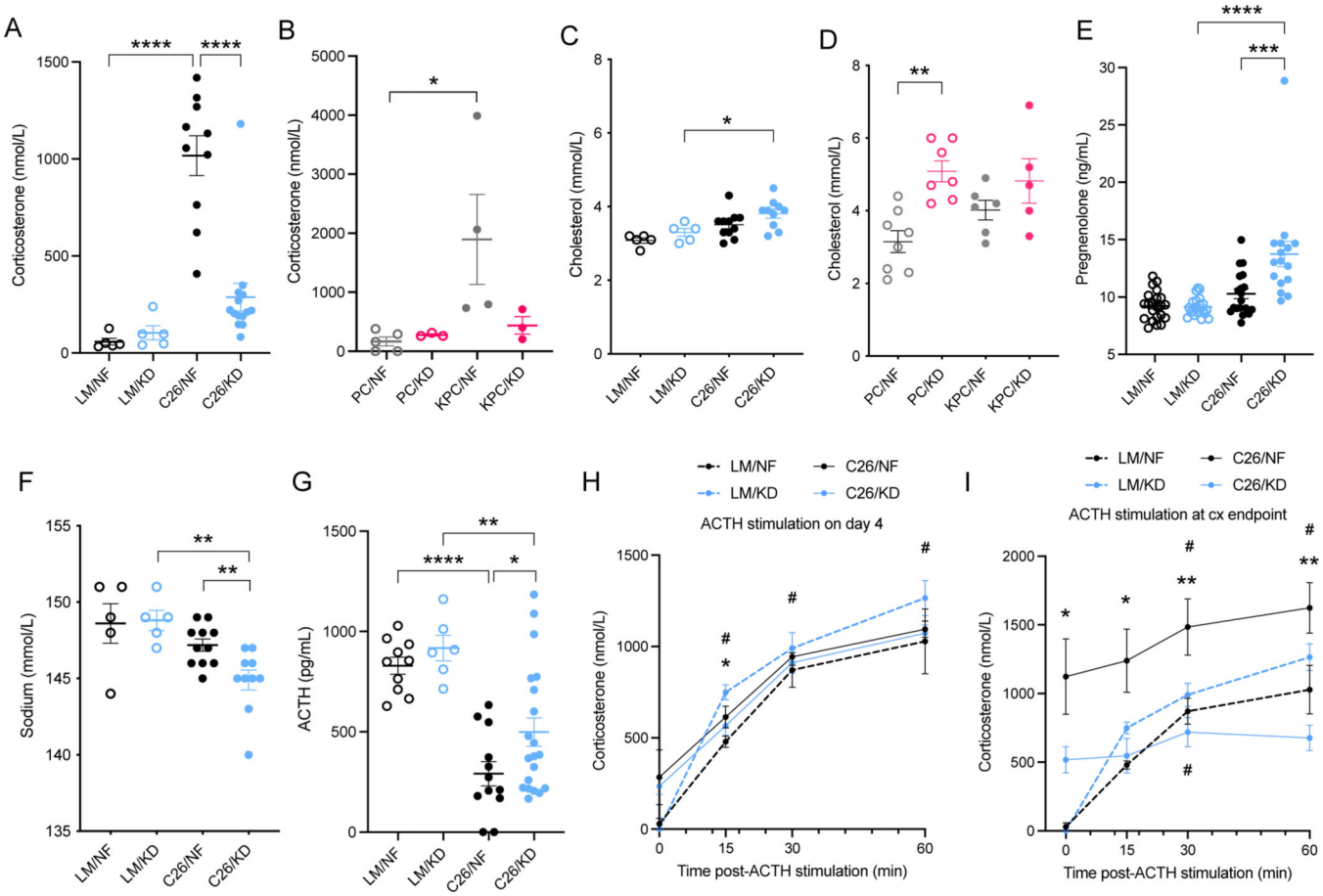

Figure 3. KD induces relative corticosterone deficiency in C26-tumor bearing mice.

(A-B) Plasma corticosterone levels in cachectic C26 and LM mice (n=5 LM, n=10–14 C26) (A) and cachectic KPC and PC mice (n=3–5) (B) fed KD or NF. (C-D) Plasma cholesterol levels in cachectic C26 and LM mice (n=5 LM, n=10–11 C26) (C), and in cachectic KPC and PC mice (n=5–8) (D) fed KD or NF. (E-G) Pregnenolone (n=16–22) ©, sodium (n=5 LM, n=10–11 C26) (F) and ACTH (n=6–10 LM, n=12–20 C26) (G) levels in plasma of cachectic C26 and LM mice on KD or NF. (H-I) Synacthen test in C26 and LM mice 4 days after diet change (n=4–5) (H), and in cachectic C26 and LM mice at endpoint (n=5–8) (I). One-way ANOVA with Tukey's correction for post hoc testing was used in (A-G). Two-way ANOVA statistical tests with Tukey's correction for post hoc comparisons were performed in (H-I). # p-value < 0.05 compared to time = 0.

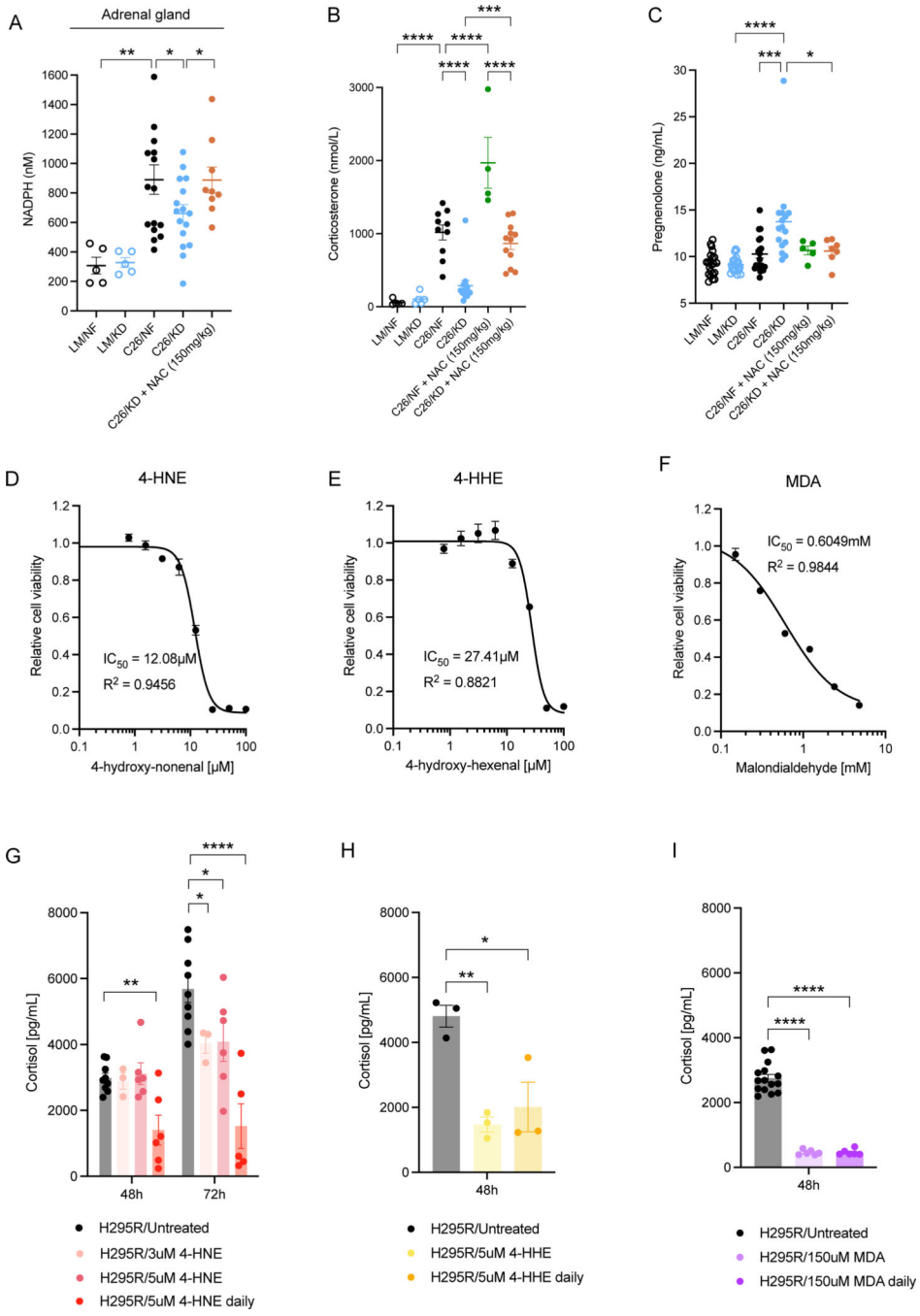

Figure 4. NAC rescues adrenal function *in vivo* and LPPs suppress cortisol production *in vitro*.
(A) NADPH quantification in the adrenal glands of C26 and LM mice fed KD or NF, and C26 mice fed KD treated with NAC (n=5 LM, n=9–16 C26). (B-C) Corticosterone (n=5–14) (B) and pregnenolone (n=5–21) (C) levels in plasma of C26 and LM mice fed KD or NF, untreated or treated with NAC. (D-F) Viability of H295R cells treated with 4-HNE (D), 4-HI© or MDA (F) (n=3 independent experiments) relative to vehicle-treated control cells. (G-I) Cortisol levels upon exposure of H295R cells to 4-HNE (n=3–6) (G), 4-HHE (n=3–6) and MDA (n=6–15) (I).

One-way ANOVA with Tukey’s correction for post hoc testing was used in (A-C, G-I).

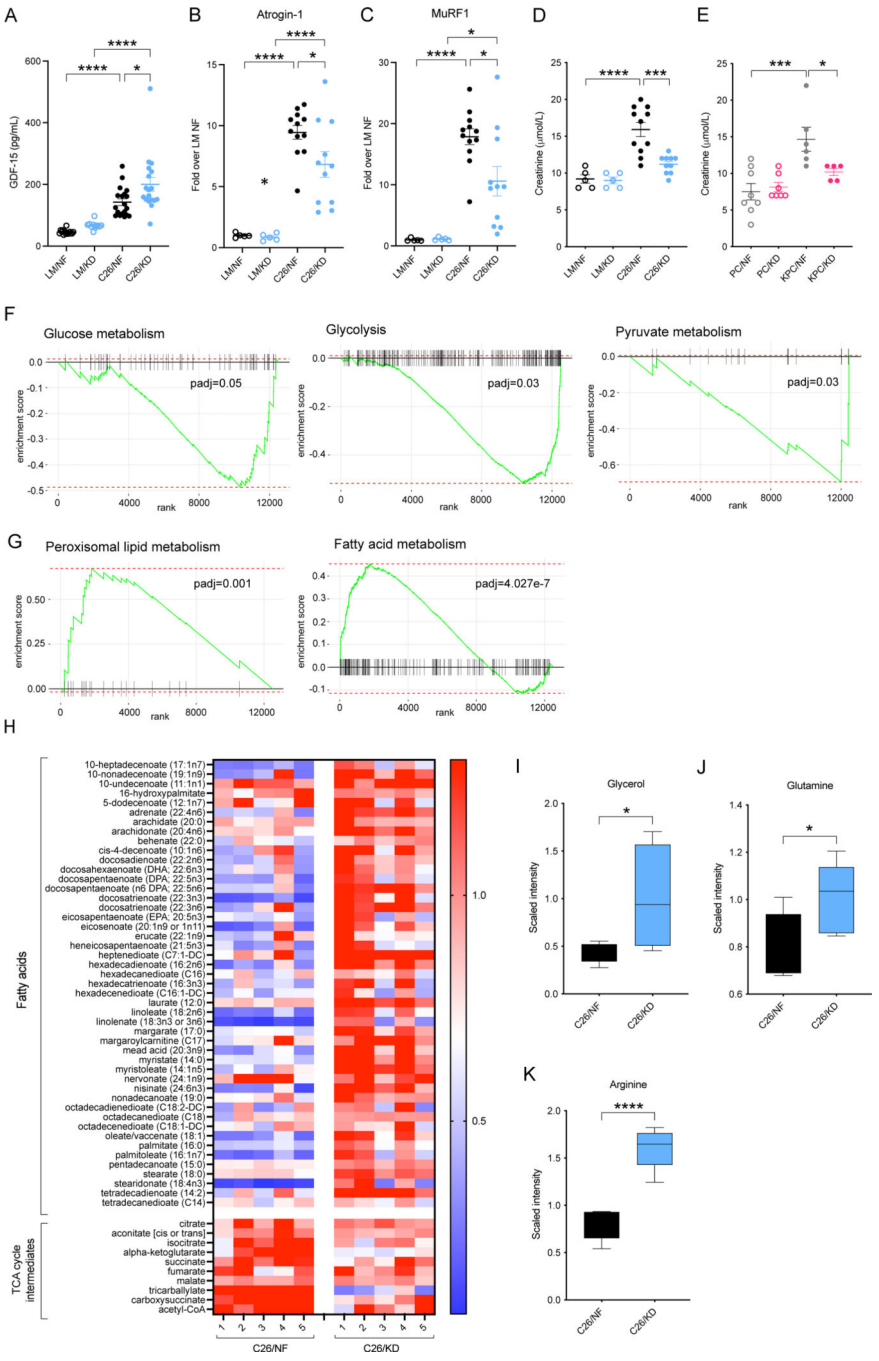

Figure 5. Metabolic adaptation in the context of cachexia is impaired in KD-fed tumor-bearing mice.

(A) Plasma levels of GDF-15 in C26 and LM mice fed KD or NF (n=11–19). (B-C) mRNA levels of the E3 ligases Atrogin-1 (B) and MuRF1 (C) in the quadriceps of C26 and LM mice fed KD or NF (n=5 LM, n=12 C26). (D-E) Plasma creatinine levels in C26 and LM mice (n=5 LM, n=9–10 C26) (D), and KPC and PC mice (n=5–8) (E) fed either KD or NF. (F-G) GSEA analysis of downregulated (F) and upregulated (G) pathways in KD-fed C26 mice compared to those NF-fed (n=5). (H) Heatmap of metabolites in C26 mice fed

KD or NF (n=5). (I-K) Quantification by UPLC-MS/MS of the main TCA cycle substrates: glycerol (I), glutamine (J), and arginine (K), in tumors of C26 mice fed KD or NF (n=6). One-way ANOVA with Tukey's correction for post hoc testing was used in (A-E). Statistical analysis in (F-G) is described in Methods. Statistical differences in (I-K) were examined using an unpaired two-tailed Student's t-test with Welch's correction.

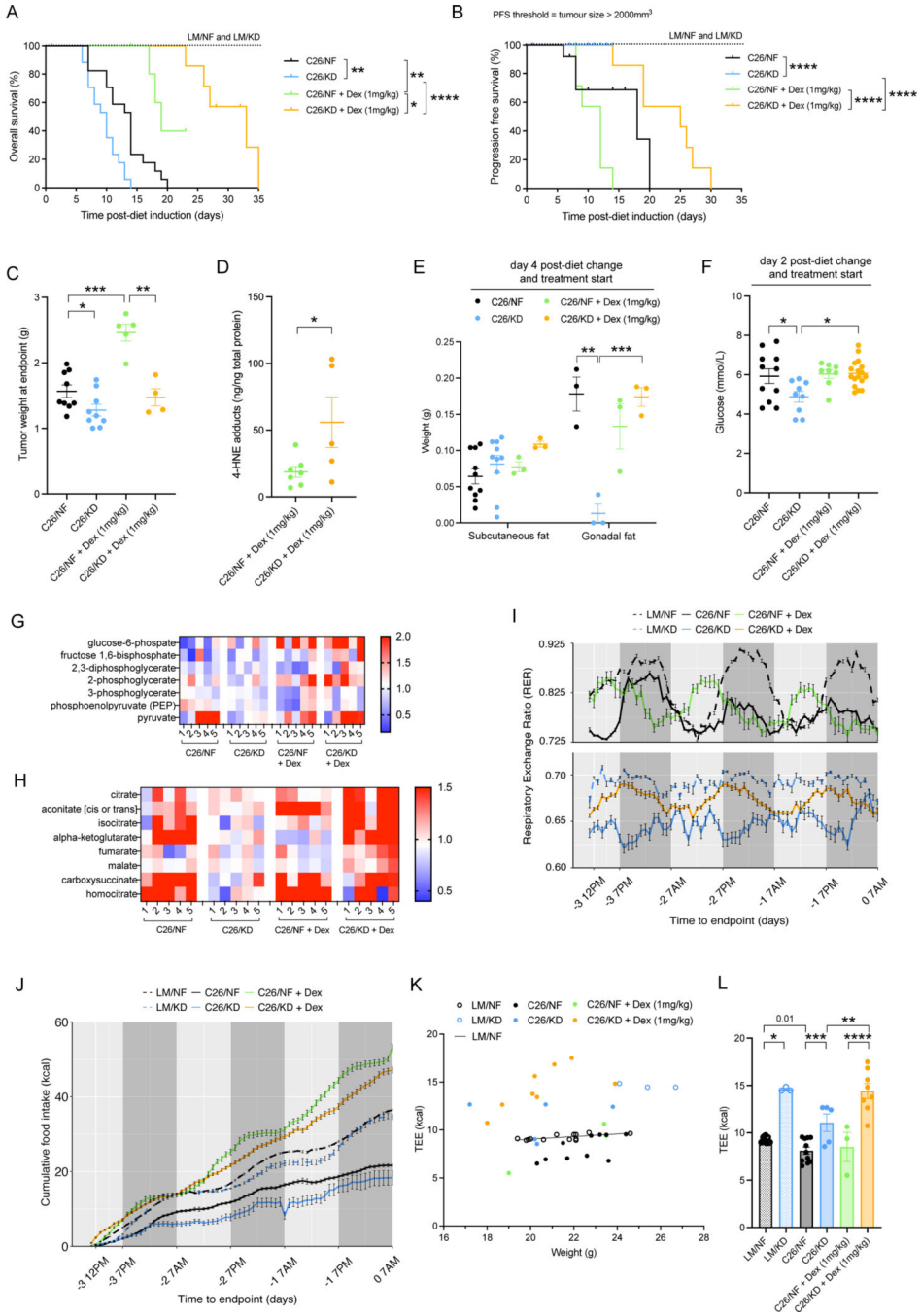

Figure 6. Dexamethasone treatment extends survival and improves metabolic adaptation of C26 mice fed KD.

(A-B) OS (A) and PFS (B) of C26 mice fed KD or NF, untreated or treated with Dexamethasone, and LM mice fed with either diet (n=7 LM, n=17–18 C26, n=7 C26 + Dex). (C) Tumor weight at endpoint in C26 mice fed KD or NF, untreated or treated with Dexamethasone (n=5–9). (D) Quantification of 4-HNE adducts in tumor lysates from C26 mice treated with Dex and fed KD or NF (n=5–7). (E) Quantification of fat tissue in C26 mice fed KD or NF, untreated or treated with Dexamethasone, 4 days after diet change and treatment start (n=3–10). (F) Plasma glucose levels in C26 mice fed KD or NF, untreated or

treated with Dexamethasone, 2 days after diet change and treatment start (n=8–17). (G-H) Quantification by UPLC-MS/MS of metabolites involved in gluconeogenesis (G) and the TCA cycle (H) in livers of C26 mice on either KD or NF diets, untreated or treated with Dexamethasone (n=5). (I) RER during the last 4 days before endpoint in LM and C26 mice, untreated or treated with Dexamethasone, fed KD or NF (n=7). (J) Calorie intake during the last 4 days before endpoint in LM and C26 mice, untreated or treated with Dexamethasone, fed KD or NF (n=7). (K-L) Scattergraph (K) and group average (L) total energy expenditure (TEE) in LM and cachectic C26 fed KD or NF, untreated or treated with Dexamethasone (n=3–11)

Overall survival (OS): time until mice reach >15% bodyweight loss. Progression-Free Survival (PFS): time until tumor size reaches > 2000 mm^3. Kaplan–Meier curves in (A-B) were statistically analyzed by using the log-rank (Mantel–Cox) test. One-way ANOVA with Tukey's correction for post hoc testing was used in (C, E, F). Unpaired two-tailed Student's t-test was used in (D). Analysis in (G-H) is described in Methods. One-way ANCOVA was conducted to determine statistical significances in (K-L) on TEE controlling for weight.

Key resources table

REAGENT or RESOURCE	SOURCE	IDENTIFIER
Antibodies		
anti-human/mouse Myeloperoxidase (MPO)	R&D Systems	Cat. #AF3667; RRID:AB_2250866
Donkey anti-Goat IgG (H+L) Alexa Fluor 633	Thermo Fisher	Cat. #A-21082; RRID:AB_10562400
anti-Ki67	Thermo Fisher	Cat. #14-5698-82; RRID:AB_10854564
anti-mouse CD45 Alexa Fluor 700	BioLegend	Cat. #103127; RRID:AB_493714
anti-mouse CD45 FITC	Thermo Fisher	Cat. #11-0451; RRID:AB_465049
anti-mouse CD3ε APC/Cy7	BioLegend	Cat. #100329; RRID:AB_1877171
anti-mouse CD4 PerCP/Cyanine 5.5	BioLegend	Cat. #100433; RRID:AB_893330
anti-mouse CD8a Brilliant Violet 510TM	BioLegend	Cat. #100751; RRID:AB_2561389
anti-mouse CD11b Brilliant Violet 605TM	BioLegend	Cat. #101257; RRID:AB_2565431
anti-mouse Ly-6G/Ly-6C Alexa Fluor 700	BioLegend	Cat. #108421; RRID:AB_493728
anti-mouse CD69 FITC	BioLegend	Cat. #104505; RRID:AB_313108
anti-mouse CD152 PE/Cy7	BioLegend	Cat. #106313; RRID:AB_2564237
anti-mouse CD274 Brilliant Violet 421TM	BioLegend	Cat. #124315; RRID:AB_10897097
anti-mouse CD279 PE/Dazzle 594	BioLegend	Cat. #109115; RRID:AB_2566547
anti-mouse F4/80 FITC	BioLegend	Cat. #123107; RRID:AB_893500
Rabbit anti-BAX mAb	Proteintech	Cat. #50599-2-Ig; RRID:AB_2061561
Rabbit β-Actin mAb	Cell Signaling	Cat. #4967; RRID:AB_330288
Rabbit Caspase-3 (D3R6Y) mAb	Cell Signaling	Cat. #14220; RRID:AB_2798429
Goat Anti-Rabbit IgG H&L (HRP)	Abcam	Cat. # ab205718; RRID:AB_2819160
Chemicals, peptides, and recombinant proteins		
Dexamethasone 21-phosphate disodium salt	Sigma-Aldrich	Cat. #D1159
N-Acetyl-L-cysteine	Sigma-Aldrich	Cat. #A9165
Sodium Chloride (NaCl) 0.9% sterile saline	Thermo Fisher	Cat. #Z1377
Liproxstatin-1	Selleck Chemicals	Cat. #S7699
RSL3 ((1S,3R)-RSL3)	MedChemExpress	Cat. #HY-100218A
Dimethyl Sulfoxide (DMSO)	Cell Signaling	Cat. #12611S
Polyethylene glycol 300 (PEG300)	Selleck Chemicals	Cat. #S6704
ACTH	ProSpec	Cat. #HOR-279
2x Lysis buffer	RayBiotech	Cat. #AA-LYS-16ml
Protease Inhibitor Cocktail	RayBiotech	Cat. #AA-PI
Phosphatase Inhibitor Cocktail Set I	RayBiotech	Cat. #AA-PHI-I
Formalin	Sigma-Aldrich	Cat. # HT501128-4L
Propylene Glycol	Sigma-Aldrich	Cat. #P4347
Oil Red O	Sigma-Aldrich	Cat. #O0625-25G
Hematoxylin and Eosin Kit	Abcam	Cat. #ab245880
Methanol	VWR	Cat. #BDH1135-4LP

REAGENT or RESOURCE	SOURCE	IDENTIFIER
Paraformaldehyde	Thermo Fisher	Cat. #50-980-495
Fetal Bovine Serum (FBS)	Thermo Fisher	Cat. #10-438-026
RPMI-640	Thermo Fisher	Cat. #11-875-093
Penicillin-Streptomycin	Thermo Fisher	Cat. #15-140-122
Trypsin-EDTA (0.5%)	Thermo Fisher	Cat. #15400054
DMEM:F12	ATCC	Cat. #30-2006
Nu-Serum I	Corning	Cat. #355100
ITS+ Premix	Corning	Cat. #354352
4-hydroxynonenal (4-HNE)	Cayman Chemical	Cat. #32100
4-hydroxyhexenal (4-HHE)	Cayman Chemical	Cat. #32060
Malondialdehyde (MDA)	Sigma-Aldrich	Cat. #63287-1G-F
Trypan blue	Thermo Fisher	Cat. #15250061
Trichloroacetic acid	Sigma-Aldrich	Cat. #T9159-100G
Sulforhodamine B (SRB)	Sigma-Aldrich	Cat. #S1402-5G
Acetic acid	Sigma-Aldrich	Cat. #A6283
Collagenase I	Sigma-Aldrich	Cat. #SCR103
DNase I	Sigma-Aldrich	Cat. #04716728001
Percoll	Sigma-Aldrich	Cat. #GE17-0891-01
RBC lysis buffer	Thermo Fisher	Cat. #A1049201
RIPA buffer	Thermo Fisher	Cat. #89901
Dithiothreitol (DTT)	Thermo Fisher	Cat. #A39225
Blotting-Grade Blocker (dry milk)	Bio-Rad	Cat. #1706404
ECL	Thermo Fisher	Cat. #32106
QIAzol Lysis Reagent	Qiagen	Cat. #79396
Critical commercial assays		
Corticosterone ELISA	IBL	Cat. #RE52211
IL-6 Quantikine ELISA	R&D	Cat. #M6000B
4-Hydroxynonenal ELISA	Novus Biologicals	Cat. #NBP2-66364
Pregnenolone ELISA	Novus Biologicals	Cat. #NBP2-68102
Progesterone ELISA	Novus Biologicals	Cat. #NBP2-60125
Leptin ELISA	Thermo Fisher	Cat. #KMC2281
ACTH ELISA	Abcam	Cat. #ab263880
NADP/NADPH-Glo™ Bioluminescent Assay	Promega	Cat. #G9081
Iron assay	Abcam	Cat. #ab83366
Lipid Peroxidation (4-HNE) Assay	Abcam	Cat. #ab238538
Cortisol Competitive ELISA	Thermo Fisher	Cat. #EIAHCOR
RNeasy Lipid Tissue Mini Kit	Qiagen	Cat. #74804
TaqMan™ RNA-to-CT™ 1-Step Kit	Thermo Fisher	Cat. #4392653
Deposited data		

REAGENT or RESOURCE	SOURCE	IDENTIFIER
RNA-sequencing data	SRA	BioProject: PRJNA961745 'KPC mice on ketogenic diet versus standard chow diet'
Data S1	This research project	Data S1 - Source Data
Experimental models: Cell lines		
C26 murine colorectal cancer		RRID:CVCL_3925
H295R human adrenocortical cancer	ATCC	Cat. #CRL-2128; RRID:CVCL_0458
Experimental models: Organisms/strains		
BALB/c	Charles River	Cat. #028
KPC (KrasG12D/+; Trp53R172H/+; P48-Cre)		
Software and algorithms		
FlowJo X (Tree Star)	FlowJo LLC	https://www.flowjo.com
CLAMS/Oxymax	Columbus Instruments	Comprehensive Lab Animal Monitoring System (CLAMS)
GraphPad Prism 9	GraphPad Software	https://www.graphpad.com
ImageJ	NIH	https://imagej.nih.gov/ij/
R studio	Posit	https://posit.co/download/rstudio-desktop/
Other		
Standard chow diet (PicoLab® Rodent Diet)	LabDiet	Cat. #5053
Ketogenic diet (KD)	Bio-Serv	Cat. #F3666
35mm Dishes with 1.5 Coverslip and 10 mm Glass Diameter	MatTek	Cat. #P35G-1.5-10-C
Nitrocellulose membranes	Thermo Fisher	Cat. #88025